The Hawaii Infrared Parallax Program. III. 2MASS J0249-0557 c

The Astronomical Journal, 156:57 (21pp), 2018 August https://doi.org/10.3847/1538-3881/aacbc2

The Hawaii Infrared Parallax Program. III. 2MASS J0249–0557 c: A Wide Planetary-mass Companion to a Low-mass Binary in the β Pic Moving Group*†

Trent J. Dupuy[1], Michael C. Liu[2], Katelyn N. Allers[3,10], Beth A. Biller[4,5,10], Kaitlin M. Kratter[6], Andrew W. Mann[7,11], Evgenya L. Shkolnik[8], Adam L. Kraus[9], and William M. J. Best[2]
[1] Gemini Observatory, Northern Operations Center, 670 N. A'ohoku Place, Hilo, HI 96720, USA
[2] Institute for Astronomy, University of Hawaii, 2680 Woodlawn Drive, Honolulu, HI 96822, USA
[3] Department of Physics and Astronomy, Bucknell University, Lewisburg, PA 17837, USA
[4] SUPA Institute for Astronomy, University of Edinburgh, Blackford Hill View, Edinburgh EH9 3HJ, UK
[5] Centre for Exoplanet Science, University of Edinburgh, UK
[6] Department of Astronomy, University of Arizona, 933 N Cherry Ave, Tucson, AZ 85721, USA
[7] Department of Astronomy, Columbia University, 550 West 120th Street, New York, NY 10027, USA
[8] School of Earth and Space Exploration, Arizona State University, Tempe, AZ 85281, USA
[9] The University of Texas at Austin, Department of Astronomy, 2515 Speedway C1400, Austin, TX 78712, USA
Received 2018 March 24; revised 2018 June 5; accepted 2018 June 9; published 2018 July 20

Abstract

We have discovered a wide planetary-mass companion to the β Pic moving group member 2MASS J02495639−0557352 (M6 VL-G) using Canada–France–Hawaii Telescope/WIRCam astrometry from the Hawaii Infrared Parallax Program. In addition, Keck laser guide star adaptive optics aperture-masking interferometry shows that the host is itself a tight binary. Altogether, 2MASS J0249−0557ABc is a bound triple system with an $11.6^{+1.3}_{-1.0}$ $M_{\rm Jup}$ object separated by 1950 ± 200 au (40″) from a relatively close (2.17 ± 0.22 au, 0.″04) pair of 48^{+13}_{-12} $M_{\rm Jup}$ and 44^{+14}_{-11} $M_{\rm Jup}$ objects. 2MASS J0249−0557AB is one of the few ultracool binaries to be discovered in a young moving group and the first confirmed in the β Pic moving group (22 ± 6 Myr). The mass, absolute magnitudes, and spectral type of 2MASS J0249−0557 c (L2 VL-G) are remarkably similar to those of the planet β Pic b (L2, $13.0^{+0.4}_{-0.3}$ $M_{\rm Jup}$). We also find that the free-floating object 2MASS J2208+2921 (L3 VL-G) is another possible β Pic moving group member with colors and absolute magnitudes similar to β Pic b and 2MASS J0249−0557 c. β Pic b is the first directly imaged planet to have a "twin," namely an object of comparable properties in the same stellar association. Such directly imaged objects provide a unique opportunity to measure atmospheric composition, variability, and rotation across different pathways of assembling planetary-mass objects from the same natal material.

Key words: binaries: close – brown dwarfs – parallaxes – planetary systems – stars: individual (2MASS J02495639-0557352, 2MASSW J2208136+292121)

1. Introduction

The formation of gas giants is a critical phase in the assembly of planetary systems from circumstellar disks. Direct imaging is a key method for studying such planets as it provides direct access to their photospheres, which can be used to probe many physical properties (e.g., composition, surface temperature, chemistry). Because direct imaging is intrinsically more sensitive to planets farther from their host stars, many planetary-mass companions have been discovered at wide separations ($\gtrsim$100 au) where it is not clear if they could have arisen from disks (e.g., see the review of Bowler 2016). In practice, this population of wide-separation companions provides an opportunity to delineate possible formation pathways, since if they formed differently than close-in gas giants, there may be evidence in their orbits or spectra (e.g., elemental abundances; Helled & Bodenheimer 2010). The widest companions ($\gtrsim 10^3$ au; e.g., Luhman et al. 2011; Naud et al. 2014; Deacon et al. 2016) offer the sharpest contrast with directly imaged planets that are on close orbits, such as 51 Eri b (13 au; Macintosh et al. 2015) and the HR 8799 system (14–68 au; Marois et al. 2008, 2010). Studying these two populations along with a third group, free-floating planetary-mass objects, like PSO J318.5338−22.8603 (Liu et al. 2013) and SDSS J1110+0116 (Gagné et al. 2015a), should offer a clearer picture of gas giant formation.

Directly imaged planets that are members of stellar associations are particularly valuable because their age and the composition of their natal material can be constrained by the entire ensemble of stars in the group. There are relatively few close-in (<100 au) imaged planets that have ages determined by being a member of a moving group or association. β Pic b (9 au; Lagrange et al. 2010) and 51 Eri b (13 au; Macintosh et al. 2015) are members of the β Pic moving group (22 ± 6 Myr; Shkolnik et al. 2017). HD 95086 b (56 au; Rameau et al. 2013) and HIP 65426 b (82 au; Chauvin et al. 2017) are members of Lower Centaurus Crux (17 ± 2 Myr; Pecaut et al. 2012). 2MASS J1207−3932 b

* Based on data obtained with WIRCam, a joint project of CFHT, Taiwan, Korea, Canada, and France, at the Canada–France–Hawaii Telescope, which is operated by the National Research Council of Canada, the Institute National des Sciences de l'Univers of the Centre National de la Recherche Scientifique of France, and the University of Hawaii.
† Data presented herein were obtained at the W.M. Keck Observatory, which is operated as a scientific partnership among the California Institute of Technology, the University of California, and the National Aeronautics and Space Administration. The Observatory was made possible by the generous financial support of the W.M. Keck Foundation.
[10] Visiting Astronomer at the Infrared Telescope Facility, which is operated by the University of Hawaii under contract NNH14CK55B with the National Aeronautics and Space Administration.
[11] NASA Hubble Fellow.

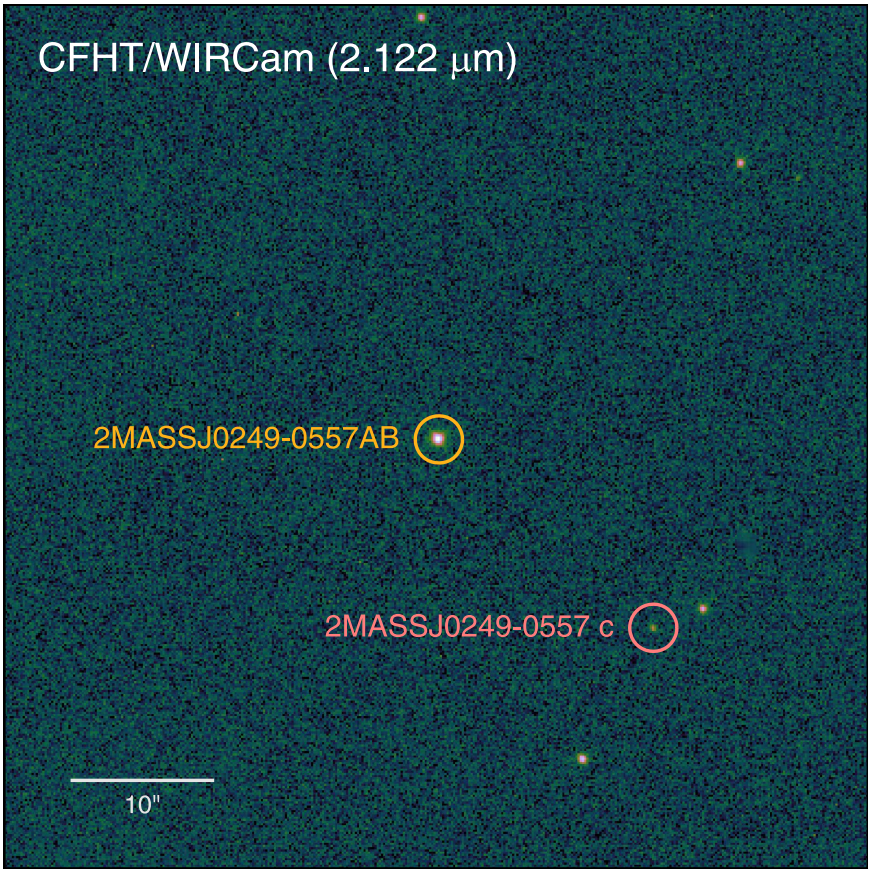

Figure 1. A 120″ × 120″ cutout from a single CFHT/WIRCam K_{H2}-band image (t_{exp} = 5 s) typical of those used in our astrometric analysis. This image was taken on 2012 August 12 UT in 0.″62 seeing and is shown at its native orientation, within 0.°1 of north up and east left, using an asinh stretch. The image is centered on the target of our parallax observations (2MASS J0249−0557AB, M6 VL-G), and the newly discovered companion is circled to the lower right. Five other unassociated reference stars are visible throughout this image, two of which are closer to 2MASS J0249−0557 c than its host star.

(41 au; Chauvin et al. 2004) is a member of the TW Hydra association (10 ± 3 Myr; Bell et al. 2015). LkCa 15 is a young Taurus member (2^{+2}_{-1} Myr; Kraus & Hillenbrand 2009) that may host one or more planets (15–20 au; Kraus & Ireland 2012; Sallum et al. 2015). And the HR 8799 system (14–68 au; Marois et al. 2008, 2010) is a proposed member of Columba (42^{+6}_{-4} Myr; Zuckerman et al. 2011; Bell et al. 2015). A few more <100 au companions have higher mass estimates that place them near or above the deuterium-fusing limit: 2MASS J0122−2439 B (52 au; Bowler et al. 2013) is a possible member of AB Doradus (150^{+50}_{-20} Myr; Bell et al. 2015), while 2MASS J0103−5515 b (84 au; Delorme et al. 2013) is a member of Tucana–Horologium (45 ± 4 Myr; Kraus et al. 2014; Bell et al. 2015).

We present here a new planetary-mass companion in the β Pic moving group discovered in seeing-limited astrometry from the Hawaii Infrared Parallax Program (Dupuy & Liu 2012; Liu et al. 2016). In addition, we have discovered that its host 2MASS J02495639−0557352 (hereinafter 2MASS J0249−0557) is actually a tight, nearly equal-flux binary using aperture-masking data obtained with Keck laser guide star adaptive optics (LGS AO). The host 2MASS J0249−0557AB was originally identified (in integrated light) as a member of the β Pic moving group by Shkolnik et al. (2017) from its proper motion and radial velocity (RV). In the following, we reaffirm this system's membership in the β Pic moving group with a parallax and new proper motion and show that the companion 2MASS J0249−0557 c is a physically bound object, making this a triple system of very low-mass objects. We discuss this unique system in the context of other β Pic members and other planetary-mass companions.

2. Observations

2.1. Canada–France–Hawaii Telescope (CFHT)/WIRCam

As part of our ongoing Hawaii Infrared Parallax Program at CFHT, we have been using the facility infrared camera WIRCam (Puget et al. 2004) to monitor 2MASS J0249−0557 in order to confirm the β Pic membership of the latest-type objects identified by Shkolnik et al. (2017). Because our observations were designed to measure the parallax of this relatively bright M6 dwarf, we used a narrow-band filter (0.032 μm bandwidth) in the K band. We refer to this filter as the K_{H2} band because it is centered at 2.122 μm, the wavelength of the H_2 1–0 S(1) line. Figure 1 shows a portion of one of our WIRCam images.

Our observing strategy and reduction pipeline are described in detail in our previous work (Dupuy & Liu 2012; Liu et al. 2016). Briefly, we measure relative astrometry of all stars above a threshold signal-to-noise ratio (S/N > 5 for this analysis), first using SExtractor (Bertin & Arnouts 1996) to compute (x, y) positions and fluxes and then our custom pipeline for the following steps. The astrometric uncertainty for a given object at a given epoch is the standard error on the mean, computed using the internal astrometric scatter across the dithered images at a single epoch. The accuracy of these

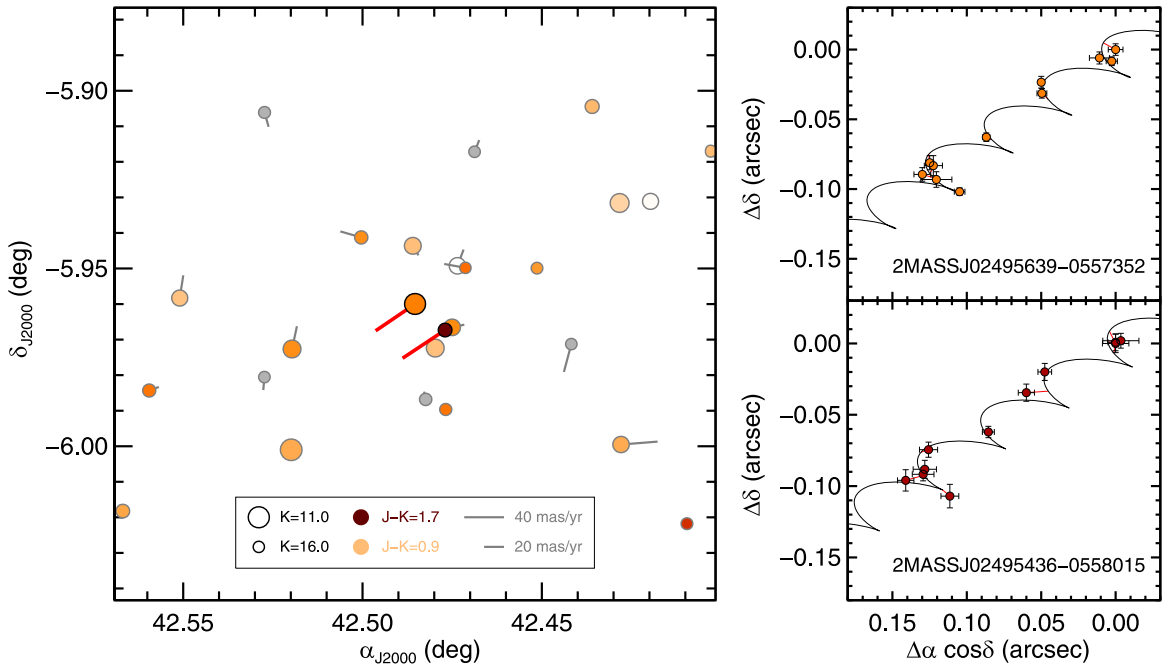

Figure 2. Left: all stars detected in our CFHT/WIRCam K_{H2}-band imaging and used in our astrometric analysis. Larger symbols indicate brighter stars, darker and redder symbols indicate redder $J - K$ colors based on 2MASS photometry (sources not in 2MASS are colored gray), and lines emanating from symbols indicate proper motion vectors where the tip of the line is the position 10^3 years from now. (Stars without lines have measured proper motions smaller than the symbol size.) The two objects in the center of the field with thick red proper motion vectors are the β Pic member 2MASS J0249−0557 and our newly identified companion. Right: relative astrometry of 2MASS J0249−0557 (top) and the companion (bottom), where the origin corresponds to the earliest epoch. The best-fit proper motion and parallax solutions, computed separately for each object, are shown as black lines. The two objects have consistent proper motions and parallaxes (Table 2), indicating that they are physically bound.

error estimates is later verified by examining the χ^2 of our final five-parameter parallax and proper motion fits to our relative astrometry. The absolute calibration of our astrometry (e.g., the pixel scale) is determined by matching low-proper-motion sources (<30 mas yr^{-1}) that also appear in an external reference catalog. In this case, all 24 of our low-proper-motion reference stars were in DR12 of the Sloan Digital Sky Survey (SDSS; Alam et al. 2015), and the rms of our astrometry compared to SDSS after performing a linear transformation was 0.″031, which we expect is dominated by the uncertainty in the SDSS relative astrometry.

Unexpectedly, we found that one of the stars in the field had a proper motion and parallax very similar to our intended target 2MASS J0249−0557 (Figure 2). This other source has the Two-Micron All-Sky Survey (2MASS) designation 2MASS J02495436−0558015, and its 2MASS photometry indicates a very red color ($J - K_S = 1.66 \pm 0.17$ mag) that would be consistent with being a later-type companion. Table 1 presents our measurements for both objects. The median relative astrometric error per epoch is 4.2 mas for 2MASS J0249−0557 (median S/N = 240) and 6.0 mas for the much fainter companion (median S/N = 15), indicating that the uncertainty in the reference grid is setting the astrometric noise floor, not the centroiding errors that scale as $\propto$FWHM/(S/N). The parallax and proper motion solutions for 2MASS J0249−0557 and the companion are given in Table 2. The relative proper motions of the two objects are consistent within the errors (1.4σ), as are the relative parallaxes (0.1σ). We show in Section 3.1 that the companion is a young L dwarf, making it very improbable that it is an unrelated object in the volume probed by our CFHT/WIRCam field of view (1.0 pc^3 within a distance limit of <70 pc). According to the 25 pc sample from W. M. J. Best et al. (2018, in preparation), the space density of L0 and later dwarfs of all ages is $\approx 1 \times 10^{-2}$ pc^{-3}, while for young objects in the same spectral type range it is $\approx 6 \times 10^{-4}$ pc^{-3}. Thus, the probability of the companion being a chance alignment is $\ll 1\%$ even before considering that it has consistent parallax and proper motion. Therefore, we find the two sources are physically associated.

We used the flux measurements reported by SExtractor (FLUX_AUTO) to compute relative photometry between 2MASS J0249−0557 and the companion at each epoch. In order to examine photometric variations in each object separately, we first computed the flux of each component relative to a well-detected nearby reference star (2MASS J02495396−0557594, $K_S = 13.28 \pm 0.04$ mag). In our K_{H2}-band data, this reference star is 1.600 ± 0.027 mag brighter than the companion and 2.179 ± 0.027 mag fainter than 2MASS J0249−0557 itself. These quoted flux ratio errors are the rms across all epochs, so neither source appears to be more variable relative to the reference star than the other. Computing the magnitude difference relative to each other instead of the reference star gives $\Delta K_{H2} = 3.780 \pm 0.032$ mag, with $\chi^2 = 14.6$ (10 dof) using the standard error at each epoch as quoted in Table 1, which again is consistent with no variability above 0.03 mag in the K_{H2} band for either object.

2.2. Keck/NIRC2 LGS AO

We first observed the M6 dwarf 2MASS J0249−0557 on 2012 January 28 UT using the LGS AO system at the Keck II telescope (Bouchez et al. 2004; van Dam et al. 2006; Wizinowich et al. 2006). We obtained several dithered K-band images with the facility near-infrared camera NIRC2 and noted

Table 1
Integrated-light K_{H2}-band Astrometry from CFHT/WIRCam

Observation date		2MASS J02495639−0557352				2MASS J02495436−0558015						
(UT)	(MJD)	R.A. (degree)	Decl. (degree)	$\sigma_{R.A.}$ (mas)	$\sigma_{Decl.}$ (mas)	R.A. (degree)	Decl. (degree)	$\sigma_{R.A.}$ (mas)	$\sigma_{Decl.}$ (mas)	Mean airmass	Seeing (arcsec)	ΔK_{H2} (mag)
2011 Aug 6	55779.6419	042.48532936	−05.95995963	4.9	4.1	042.47695124	−05.96729310	8.8	6.4	1.137	0.54	3.796 ± 0.026
2011 Sep 11	55815.5725	042.48533240	−05.95996130	6.7	4.3	042.47695026	−05.96729258	12.1	5.2	1.111	0.58	3.748 ± 0.051
2011 Oct 16	55850.4559	042.48533009	−05.95996196	3.7	3.1	042.47695126	−05.96729288	5.0	5.9	1.126	0.50	3.780 ± 0.031
2012 Aug 12	56151.6387	042.48534333	−05.95996614	2.0	4.2	042.47696454	−05.96729865	4.6	6.0	1.118	0.60	3.851 ± 0.022
2012 Oct 5	56205.5070	042.48534321	−05.95996834	3.3	3.4	042.47696800	−05.96730269	5.4	6.0	1.110	0.58	3.764 ± 0.021
2013 Oct 14	56579.5098	042.48535363	−05.95997709	2.4	3.1	042.47697513	−05.96731035	4.0	4.0	1.123	0.48	3.742 ± 0.030
2014 Jul 30	56868.6432	042.48536427	−05.95998217	2.7	5.1	042.47698636	−05.96731379	6.1	5.3	1.172	0.50	3.776 ± 0.022
2014 Oct 3	56933.5614	042.48536358	−05.95998275	6.1	7.2	042.47698706	−05.96731761	7.8	6.3	1.157	0.53	3.795 ± 0.030
2014 Oct 13	56943.4851	042.48536301	−05.95998551	10.4	5.6	042.47699064	−05.96731977	5.5	7.5	1.110	0.63	3.743 ± 0.041
2014 Oct 16	56946.4721	042.48536565	−05.95998450	5.6	4.8	042.47698737	−05.96731859	7.3	4.6	1.112	0.51	3.779 ± 0.056
2015 Jan 21	57043.2480	042.48535865	−05.95998794	3.5	2.8	042.47698235	−05.96732283	5.9	8.2	1.133	0.57	3.801 ± 0.032

Note. The quoted uncertainties correspond to relative, not absolute, astrometric errors.

Table 2
Parallax and Proper Motion from CFHT/WIRCam Astrometry

Parameter	2MASS J02495639−0557352	2MASS J02495436−0558015
R.A. at first epoch[a] (degree)	42.4853267	42.4769477
Decl. at first epoch[a] (degree)	−05.9599598	−05.9672920
Relative parallax π_{rel} (mas)	19.2 ± 2.1	18.8 ± 3.5
Relative proper motion in R.A. (mas yr^{-1})	39.4 ± 1.0	42.5 ± 1.6
Relative proper motion in Decl. (mas yr^{-1})	−27.1 ± 0.9	−28.7 ± 1.4
Absolute parallax π_{abs} (mas)	20.5 ± 2.1	20.1 ± 3.5
Absolute proper motion in R.A. (mas yr^{-1})	42.9 ± 2.0	46.0 ± 2.3
Absolute proper motion in Decl. (mas yr^{-1})	−30.2 ± 1.8	−32.0 ± 2.1
χ^2 (17 dof)	17.4	19.2
$p(\chi^2)$	0.43	0.32

Note.
[a] First observation epoch: 55779.64 MJD, 2011 August 6 UT.

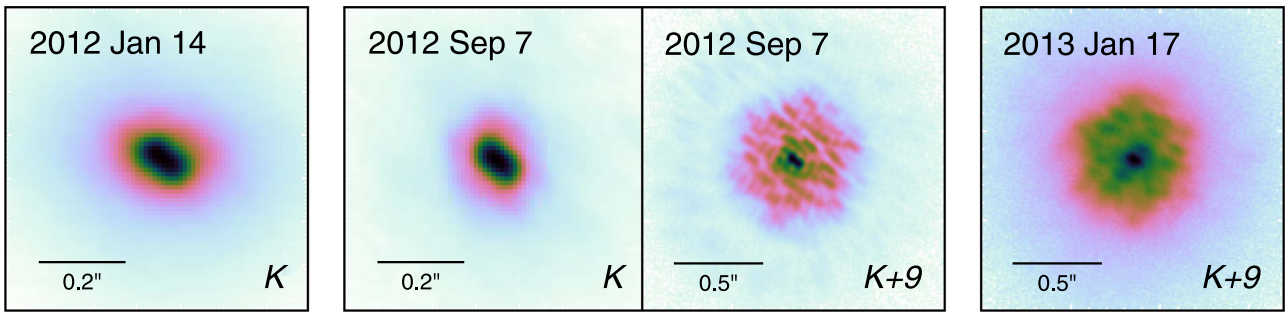

Figure 3. Keck/NIRC2 LGS AO images (left two) and nine-hole pupil-mask interferograms (right two) of 2MASS J0249−0557AB. All of these cutouts have been rotated for display purposes such that north is up and east is left and are shown with a square-root stretch. The interferogram cutouts show a larger area of the detector (i.e., they are zoomed out) compared to the direct images. We are unable to derive astrometry from the imaging data because the binary is not cleanly resolved, but analysis of both masking observations results in significant binary detections and precise astrometry. For instance, in the 2012 September 7 UT data, the imaging PSF is elongated at the same PA as the double peak in the center of the interferogram's PSF, and the masking analysis detects a binary with a separation of 44.4 ± 0.2 mas and PA of 233°.3 ± 0°.3.

an elongation in the point-spread function (PSF), but it was not clear if this was due to unstable AO correction or a marginally resolved binary. On 2012 September 7 UT, we obtained data using the nine-hole nonredundant aperture mask installed in the filter wheel of NIRC2 (Tuthill et al. 2006), in addition to more imaging in which the PSF was elongated in a fashion similar to the previous epoch. We analyzed our masking data using the same pipeline as in our previous papers (e.g., Ireland & Kraus 2008; Dupuy et al. 2009b, 2015b; Dupuy & Liu 2017). The analysis indicated a significant detection of a nearly equal-flux binary with the same PA as the PSF elongation. In order to confirm the physical association of this binary, we obtained more masking data on 2013 January 17 UT and recovered a detection at a similar separation, PA, and flux ratio. Figure 3 shows examples of all of our imaging and masking data. In computing astrometry from our NIRC2 data, we adopt the calibration from Yelda et al. (2010), as appropriate for our data taken during 2012–2013, which has a pixel scale of 9.952 ± 0.002 mas pixel^{-1} and an orientation for the detector's $+y$ axis of $-0°.252 \pm 0°.009$ east of north.[12]

[12] In our past work (e.g., Dupuy et al. 2016b; Dupuy & Liu 2017), we reported PA values with a positive offset added to the header orientation, as prescribed by Yelda et al. (2010). The offsets we used in the past were +0°.252 for Yelda et al. (2010) and +0°.262 for Service et al. (2016). However, as discussed by Bowler et al. (2018), the sign of these offsets should be negative, not positive as stated in Yelda et al. (2010).

Table 3
Keck LGS AO Astrometry of 2MASS J0249−0557AB

Observation date (UT)	Observation date (MJD)	Separation (mas)	PA (degree)	ΔK (mag)
2012 Sep 7	56177.60	44.4 ± 0.2	233°.1 ± 0°.3	0.123 ± 0.005
2013 Jan 17	56309.27	40.1 ± 0.2	237°.3 ± 0°.5	0.111 ± 0.017

At discovery, the separation of the binary was 44.4 ± 0.2 mas, and after 0.36 year it had moved inward to 40.1 ± 0.2 mas. The total motion of the secondary relative to the primary between the two epochs was $(\Delta\alpha \cos\delta, \Delta\delta) = (+1.8 \pm 0.3, +5.0 \pm 0.4)$ mas. According to our CFHT parallax solution for 2MASS J0249−0557, if the object in our Keck data were an unbound background object with zero proper motion and parallax, it would have moved $(\Delta\alpha \cos\delta, \Delta\delta) = (+19.6 \pm 3.5, +19.5 \pm 1.1)$ mas with respect to the primary. Therefore, we conclude that the observed motion is consistent with orbital motion as a physically bound binary system, since a background object would require a finely tuned and high-amplitude proper motion (≈20 mas yr^{-1}) to match our Keck LGS AO astrometry. Table 3 summarizes our measured astrometry and flux ratios for this new binary 2MASS J0249−0557AB. We note that ΔK is consistent within ≈0.01 mag and within the quoted uncertainties between the two epochs.

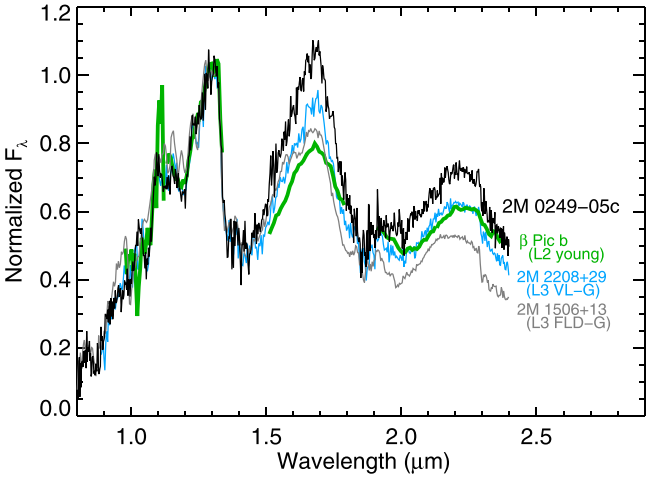

Figure 4. Near-IR IRTF/SpeX spectrum of 2MASS J0249−0557 c compared to the near-IR field standard 2MASS J1506+1321 (Kirkpatrick et al. 2010), the young (VL-G) standard 2MASS J2208+2921 (Allers & Liu 2013), and the young exoplanet β Pic b (Chilcote et al. 2017). The spectra are normalized at the peak region in the J band (1.26–1.31 μm). For the two standards, the SpeX data were taken with the 0.″5 slit (wavelength-dependent $R \approx 80$–200), and our SpeX spectrum of 2MASS J0249−0557 c was taken with the 0.″8 slit ($R \approx 50$–120). The β Pic b data come from the Gemini Planet Imager and have a spectral resolution ranging from $R \approx 35$ (Y band) up to $R \approx 75$ (K band), too coarse for AL13 gravity classification. For β Pic b, two strongly discrepant data points around 1.30 μm have been removed for plotting purposes.

2.3. NASA Infrared Telescope Facility (IRTF)/SpeX

We obtained low-resolution near-IR (0.8–2.5 μm) spectra of 2MASS J0249−0557 c on 2018 February 17 UT from IRTF located on Maunakea, Hawaii. Conditions were lightly cloudy with 0.″9 seeing. We used the facility near-IR spectrograph SpeX (Rayner et al. 1998) in prism mode with the 0.″8 slit. The wavelength-dependent resolution with this slit ranges from $R \approx 50$ in the J band to $R \approx 120$ in the K band. We oriented the field to prevent other stars from landing on the slit. This fixed PA did not correspond to the parallactic angle, but as we discuss in Section 3.1, synthetic colors derived from our spectrum agree well with 2MASS photometry, indicating that wavelength-dependent slit losses were negligible. We nodded the object along the slit in an ABBA pattern with individual exposure times of 180 s, observed over an average airmass of 1.30. We observed the A0V star HD 18571 contemporaneously for telluric calibration. The total on-source integration time was 60 minutes. All spectra were reduced using version 4.1 of the SpeXtool software (Vacca et al. 2003; Cushing et al. 2004).

2.4. APO/TripleSpec

On 2018 February 27 UT, we obtained a moderate-resolution ($R \approx 3500$) near-IR spectrum of 2MASS J0249−0557 c using TripleSpec on Apache Point Observatory's ARC 3.5 m telescope. TripleSpec (Wilson et al. 2004) is a cross-dispersed spectrograph that provides simultaneous wavelength coverage from 1.0 to 2.4 μm. Conditions during our observations were clear with ≈1.″4 seeing, which was well matched to TripleSpec's 1.″1 slit. We observed 2MASS J0249−0557 c for a total on-source integration time of 80 minutes at an average airmass of 1.83. Over the course of our observations, the orientation of the slit was continuously updated to the parallactic angle to minimize atmospheric dispersion. Immediately following our observation, we observed the A0V star HD 25792 at an airmass of 1.86 to correct for telluric absorption. All spectra were reduced using a modified version of SpeXtool 4.1 (Vacca et al. 2003; Cushing et al. 2004).

3. Results

3.1. Spectral Classification and Photometry

Figures 4–6 show the spectrum of 2MASS J0249−0557 c compared to objects of similar near-IR spectral type. The low-gravity nature of the object is seen clearly in the H-band continuum shape (triangular compared to field objects), K-band continuum shape (redder continuum peak and different curvature of the blueward continuum), VO 1.08 μm absorption (stronger), and FeH 0.99 μm absorption (weaker), as discussed, for example, in Allers & Liu (2013, hereinafter AL13). To assign a spectral type and to assess the gravity for 2MASS J0249−0557 c, we follow the near-IR classification methods of AL13. This approach uses a combination of qualitative visual typing with quantitative measurement of flux indices to determine a spectral type. The AL13 approach then determines a gravity classification using flux indices and equivalent widths of gravity-sensitive features.

For visual typing, we compare our SpeX J- and K-band spectra to near-IR spectroscopic standards for field (high-gravity [FLD-G]) objects from Kirkpatrick et al. (2010) and for young (low-gravity [VL-G]) objects from AL13. Following the prescription of AL13, in each bandpass we normalize the fluxes of 2MASS J0249−0557 c and the spectroscopic standards prior to visual comparison.[13] The near-IR spectrum of 2MASS J0249−0557 c matches the L3 VL-G standard 2MASSW J2208136+292121 (hereinafter 2MASS J2208+2921) very well, even for the H-band spectrum, though this was not used for typing.

For index-based analysis, we use the approach of Aller et al. (2016), which calculates the AL13 indices and includes a Monte Carlo estimation of the measurement errors. Combining spectral types calculated from AL13's four gravity-sensitive indices (L2.4 ± 1.2, L2.1 ± 1.0, L0.5 ± 1.2, and L2.0 ± 1.0) with our visual classification of the SpeX J- and K-band spectra (L3 ± 1 and L3 ± 1, respectively), we assign a spectral type of L2 ± 1.

From the low-resolution SpeX spectrum, we find an AL13 gravity score of 1222, which represents the gravity inferred from four spectral features, leading to a gravity classification of VL-G. We also used our moderate-resolution TripleSpec spectrum to calculate the AL13 low-resolution gravity-sensitive indices as well as the additional AL13 indices and equivalent widths available at moderate resolution. We find an AL13 gravity score of 2222 for our TripleSpec spectrum, confirming the VL-G classification determined from our lower resolution SpeX spectrum. We assign a final classification of L2 ± 1 VL-G.

We also use our spectrum of 2MASS J0249−0557 c along with the published integrated-light SpeX spectrum of 2MASS J0249−0557AB from Shkolnik et al. (2017) to synthesize photometry on the MKO system. We first synthesize offsets for both objects between the MKO and 2MASS

[13] The AL13 approach of normalizing each bandpass separately prior to visual comparison, rather than normalizing the entire near-IR spectrum, is conceptually identical to the classification system recently proposed by Cruz et al. (2018). Their study does include the H band for visual classification, which AL13 does not, and also has a few differences in the spectroscopic standards.

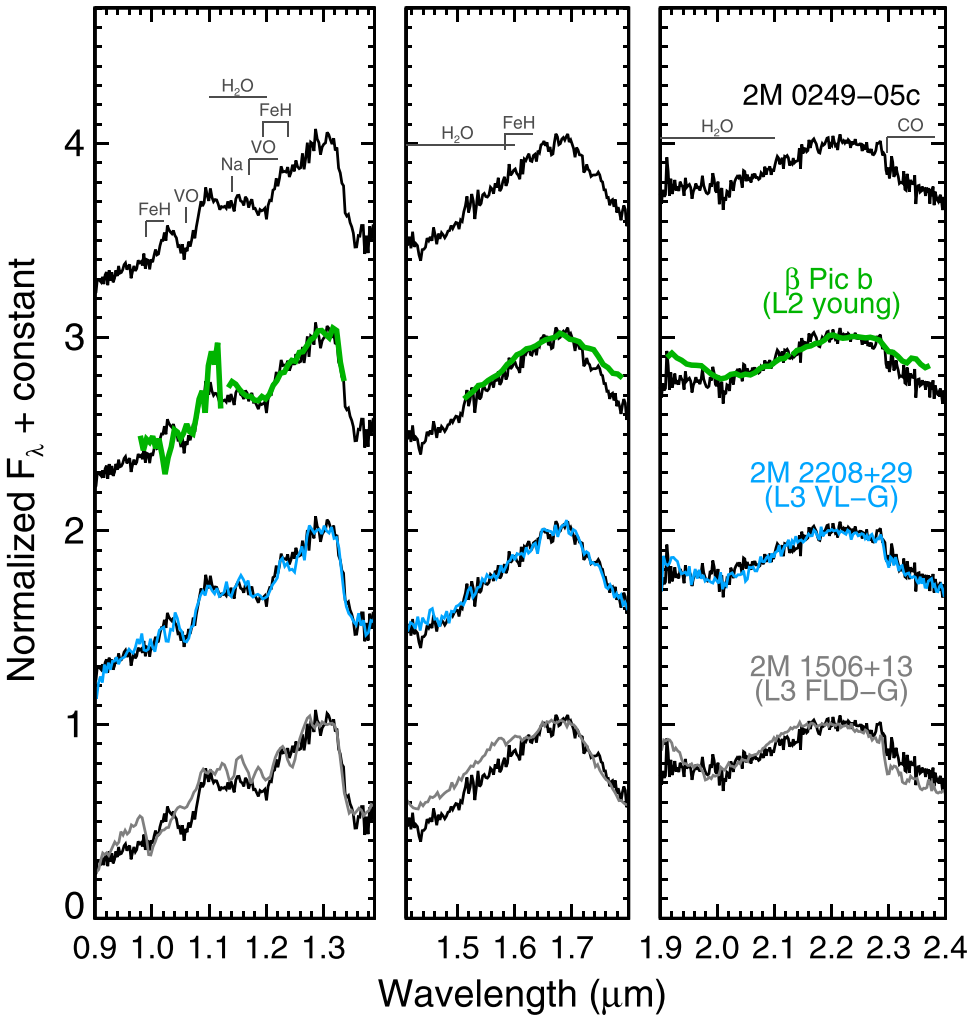

Figure 5. Comparison of the same spectra as in Figure 4, now with each bandpass separately normalized. The 2MASS J0249−0557 c spectrum is plotted four times. The L3 VL-G standard 2MASS J2208+2921 provides an excellent match in all bands, with β Pic b also being quite similar.

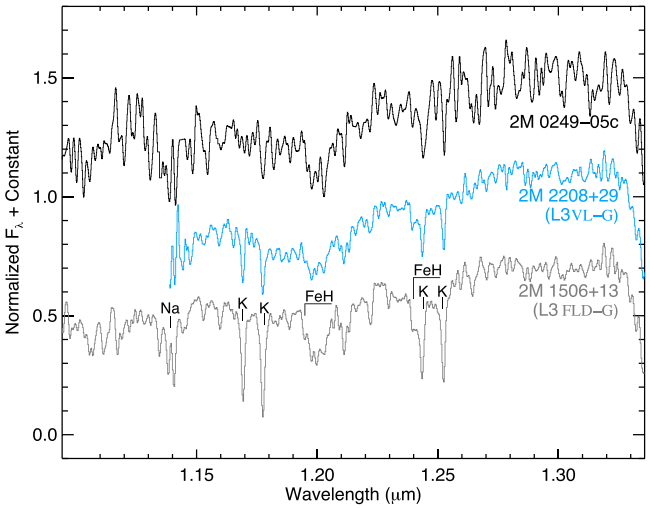

Figure 6. *J*-band APO/TripleSpec spectrum of 2MASS J0249−0557 c compared to the spectra of the near-IR field standard 2MASS J1506+1321 (Cushing et al. 2005) and the young (VL-G) object 2MASS J2208+2921 (Martin et al. 2017). All spectra have been smoothed to $R \approx 1200$, are normalized by their median flux from 1.27 to 1.31 μm, and are then offset by a constant. The spectrum of 2MASS J0249−0557 c shows the weak K I, Na I, and FeH absorption features indicative of a young, low-gravity object.

photometric systems in each bandpass, as well as the offset between broadband K and the narrow K_{H2} bandpass used in our CFHT/WIRCam imaging. We used 2MASS photometry (Cutri et al. 2003) to flux calibrate the spectrum of 2MASS J0249−0557AB, and then we used our CFHT flux ratio ($\Delta K_{H2} = 3.780 \pm 0.032$ mag) to flux calibrate the spectrum of 2MASS J0249−0557 c. In this process, we checked our synthesized 2MASS JHK_S magnitudes against the 2MASS photometry of 2MASS J0249−0557 c and found good agreement, $p(\chi^2) = 0.35$, but with our synthesized photometry having much smaller errors. The resulting synthesized *JHK* photometry on the MKO system for both objects is given in Table 4. As in our previous work with synthesized photometry (Dupuy & Liu 2012), we consider the errors on photometric system offsets negligible compared to the uncertainties in 2MASS photometry, and we adopt 0.05 mag errors on synthesized magnitudes when no direct photometry is available.

3.2. Bolometric Fluxes

In order to ultimately derive physical properties for the components of the 2MASS J0249−0557 system, we must first estimate their bolometric fluxes. We use the procedure

Table 4
Properties of the 2MASS J0249−0557 System

Property	2MASS J0249−0557A	2MASS J0249−0557B	2MASS J0249−0557 c	Notes
Distance (pc)		$48.9^{+4.4}_{-5.4}$		1
$m - M$ (mag)		$3.44^{+0.21}_{-0.23}$		1
Age (Myr)		22 ± 6		2
Spectral type		M6 VL-G	L2 VL-G	3
J (mag)		11.885 ± 0.027	16.64 ± 0.06	4
H (mag)		11.410 ± 0.026	15.61 ± 0.06	4
K (mag)	11.73 ± 0.03	11.85 ± 0.03	14.78 ± 0.03	4
$J - K$ (mag)		0.852 ± 0.034	1.86 ± 0.05	4
$H - K$ (mag)		0.376 ± 0.033	0.83 ± 0.05	4
$W1$ (mag)		10.844 ± 0.023	14.125 ± 0.034	5
$W2$ (mag)		10.597 ± 0.020	13.588 ± 0.036	5
$W1$ − W2 (mag)		0.247 ± 0.030	0.54 ± 0.05	5
m_{bol} (mag)	14.65 ± 0.05	14.77 ± 0.05	18.18 ± 0.06	6
log (L_{bol}) [$L_\odot$]	−2.59 ± 0.09	−2.64 ± 0.09	−4.00 ± 0.09	6
Mass (M_{Jup})	48^{+13}_{-12}	44^{+14}_{-11}	$11.6^{+1.3}_{-1.0}$	7
Relative properties of AB–c				
Separation (au)		1950 ± 200		8
Separation (arcsec)		39.″959 ± 0.″005		8
PA (degree)		228.°649 ± 0.°013		8
ΔK_{H2} (mag)		3.780 ± 0.032		8
Relative properties of A–B				
Separation (au)		2.17 ± 0.22	...	9
Separation (arcsec)		0.″0444 ± 0.″0002	...	9
PA (degree)		233.°1 ± 0.°3	...	9
ΔK (mag)		0.123 ± 0.005	...	9

Note. (1) Computed directly from our measured parallax; (2) lithium-depletion boundary age from Shkolnik et al. (2017); (3) infrared types on the Allers & Liu (2013) system; (4) MKO photometry synthesized from SpeX spectra, where the integrated-light spectrum of 2MASS J0249−0557AB was flux calibrated using its 2MASS photometry and 2MASS J0249−0557 c was flux calibrated from our CFHT/WIRCam K_{H2}-band photometry; (5) AllWISE photometry (Cutri et al. 2014); (6) for 2MASS J0249−0557AB, we used its integrated-light m_{bol} and observed K-band flux ratio, and we assumed that the difference in K-band bolometric corrections for A and B is negligible; (7) estimated from Baraffe et al. (2015) models for 2MASS J0249−0557AB and Saumon & Marley (2008) hybrid models for 2MASS J0249−0557 c; (8) from CFHT/WIRCam imaging; (9) Keck/NIRC2 masking detection at discovery epoch 2012 September 7 UT.

from Mann et al. (2015), which we briefly summarize here. For both 2MASS J0249−0557AB (in integrated light) and 2MASS J0249−0557 c, we compiled optical and IR photometry from SDSS-DR14 (Abolfathi et al. 2017), 2MASS, and the *Wide-field Infrared Survey Explorer* (*WISE*; Wright et al. 2010). We also used the MKO K-band photometry of 2MASS J0249−0557 c from Section 3.1 that is based on our CFHT/WIRCam imaging. For each object, we compared all available photometry to synthetic magnitudes computed from either observed, template, or model spectra. For 2MASS J0249−0557AB, we used our IRTF/SpeX spectrum and a template optical spectrum of the M6 VL-G object 2MASS J03363144−2619578 obtained with SNIFS (A. W. Mann et al. 2018, in preparation). For 2MASS J0249−0557 c, we used the combination of our IRTF/SpeX spectrum, an optical spectrum from SDSS, and a BT-Settl model (Allard et al. 2011) in regions not covered by the empirical spectra. To compute synthetic magnitudes from each spectrum, we used appropriate filter profiles and zero points (e.g., Cohen et al. 2003; Jarrett et al. 2011). Spectra were then scaled to match all available photometry, using the overlapping wavelengths of the IR and optical spectra (0.75–0.85 μm) as an additional constraint.

Figure 7 shows final calibrated spectra. To compute bolometric fluxes (f_{bol}), we integrated over these joined and absolutely calibrated spectra. We derived f_{bol} errors accounting for uncertainties in the spectral flux calibration, filter zero points, and Poisson errors in the observed photometry and spectra, yielding final values of $(1.35 \pm 0.07) \times 10^{-12}$ erg cm^{-2} s^{-1} for 2MASS J0249−0557 c and $(6.56 \pm 0.29) \times 10^{-11}$ erg cm^{-2} s^{-1} for 2MASS J0249−0557AB in integrated light. Table 4 summarizes these results in terms of apparent bolometric magnitudes (m_{bol}) so that future improvements in distance measurements can be readily applied. Our integrated-light magnitude for 2MASS J0249−0557AB of $m_{bol} = 13.96 \pm 0.05$ mag is in good agreement with the value of 13.92 ± 0.02 mas determined from photometry alone by Shkolnik et al. (2017).

3.3. Membership Assessment for 2MASS J0249−0557

Our new parallax and independently measured proper motion allow us to reexamine the membership of 2MASS J0249−0557AB in the β Pic moving group, as the original analysis by Shkolnik et al. (2017) used a less precise proper motion, did not have a parallax, and did not know it was an unresolved binary. In fact, even our proper motion measurement could be influenced by photocenter motion due to the binary orbit of 2MASS J0249−0557AB. Over short time baselines, long-term orbital motion can cause systematic offsets

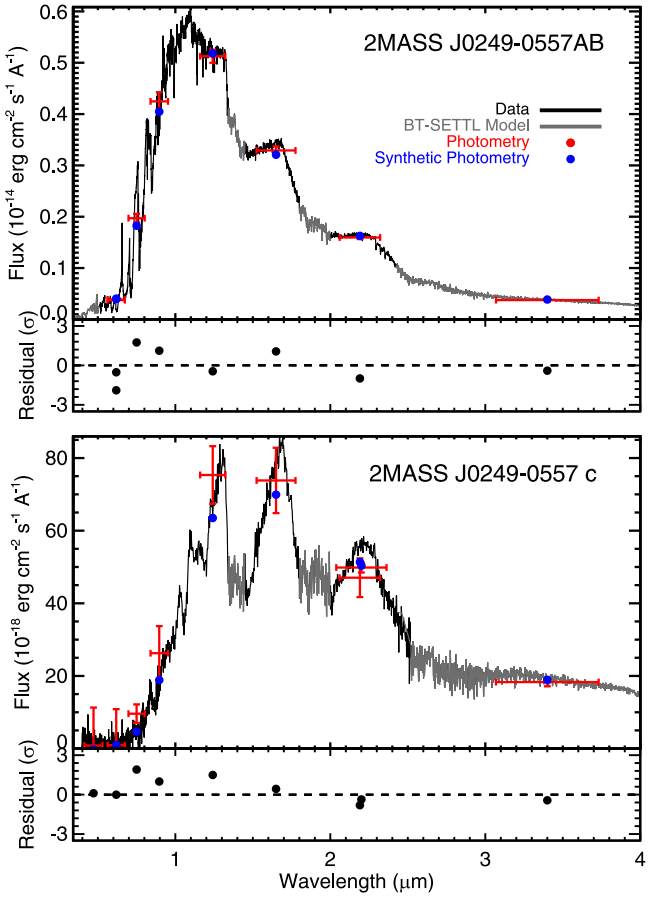

Figure 7. Absolutely flux-calibrated spectra that we use to compute bolometric fluxes ($f_{\rm bol}$). Black indicates directly observed spectra, and gray indicates wavelength regions that are likely to have high telluric contamination or that are beyond the observations, which we have filled in using BT-Settl atmospheric models. Red points are literature photometry, where y-axis error bars correspond to reported measurement uncertainties and x-axis error bars indicate the width of the filter. Blue points show synthetic photometry computed from the displayed spectrum. The bottom panel shows residuals (observed minus synthetic photometry) in units of standard deviations.

in measured proper motions (e.g., see Section 2.4.1 of Dupuy & Liu 2012), while parallaxes are not commonly affected systematically. Fortunately, the companion has proper-motion precision similar to 2MASS J0249−0557AB but is less likely to harbor unknown systematic errors due to orbital motion, as it is not known to be a binary and is marginally fainter than average for its spectral type (Section 3.5). Therefore, in the following kinematic analysis, we use the proper motion of 2MASS J0249−0557 c but the more precise parallax of 2MASS J0249−0557AB.

3.3.1. Binary Influence on the RV

We consider the possibility that the unresolved binarity of 2MASS J0249−0557AB may have influenced the Shkolnik et al. RV measured in optical integrated light. The velocity difference of the two components was not large enough relative to $v\sin(i)$ to appear as a double-lined spectroscopic binary, but the line centroids could have been shifted by the binary orbit. If this were an exactly equal-flux, equal-mass binary, then the spectral lines would broaden slightly while remaining centered at the system velocity. But for an arbitrary flux ratio and mass ratio, the flux-weighted centroid shift of the spectral lines away from the system velocity is

$$\Delta {\rm RV}_{\rm orb}\left(\frac{F_{\rm A}}{F_{\rm tot}}\frac{M_{\rm B}}{M_{\rm tot}} - \frac{F_{\rm B}}{F_{\rm tot}}\frac{M_{\rm A}}{M_{\rm tot}}\right),$$

where $\Delta {\rm RV}_{\rm orb}$ is the RV difference between the two components at a given epoch. As described in Section 3.6, we estimate a mass ratio of $M_{\rm B}/M_{\rm A} = 0.9$ from evolutionary models at the age of the β Pic moving group. (The mass ratio would be negligibly different at older field ages.) Using our Keck infrared flux ratio of $\Delta K = 0.123 \pm 0.005$ mag with the BT-Settl evolutionary model magnitudes (Allard et al. 2011), we estimate an r-band flux ratio of $F_{\rm B}/F_{\rm A} = 0.75$ (0.31 mag), and this is also essentially the same for young and old ages. Thus, the factor by which $\Delta {\rm RV}_{\rm orb}$ must be multiplied to compute the expected shift in the integrated-light RV (i.e., the term in parentheses in the equation above) is 0.045 assuming β Pic membership.[14]

We consider the possibilities of low- and high-eccentricity orbits and conservatively assume an edge-on orbit, which would produce maximal RVs. As described below, the detection of lithium implies that the system must be younger than ≈100 Myr, corresponding to masses of 0.08–0.11 $M_\odot$ for the components of 2MASS J0249−0557AB, depending on the age, so we assume a system mass of 0.2 $M_\odot$ to convert semimajor axis to orbital period. To estimate the semimajor axis from the observed projected separation, we use the conversion factors calculated by Dupuy & Liu (2011) for very low-mass binaries. Because this binary was discovered near the resolution limit of our Keck imaging, we use the value of $a/\rho = 0.85$ corresponding to severe discovery bias. Thus our measured separation of 2.17 ± 0.22 au implies a semimajor axis of 1.8 ± 0.3 au and orbital period of 5.4 years for a system mass of 0.2 $M_\odot$. In this case, the median $\Delta {\rm RV}_{\rm orb}$ is 6.6 km s^{-1} for low eccentricity ($e = 0.2$) and 2.9 km s^{-1} for high eccentricity ($e = 0.8$). The maximum possible $\Delta {\rm RV}_{\rm orb}$ values for these orbits are 12 km s^{-1} and 30 km s^{-1}, respectively. A fractional shift of 0.045 × $\Delta {\rm RV}_{\rm orb}$ implies typical deviations from systemic velocity in the integrated-light spectral lines of 0.30 km s^{-1} (up to 0.55 km s^{-1}) for low eccentricity and 0.13 km s^{-1} (up to 1.3 km s^{-1}) for high eccentricity, depending on orbital phase. The integrated-light RV of 14.42 ± 0.44 km s^{-1} from Shkolnik et al. (2017) was measured on 2010 December 31 UT, 1.69 years prior to our first Keck LGS AO astrometry. Thus we cannot rule out a scenario in which 2MASS J0249−0557AB is an eccentric binary that would have been going through periastron passage (i.e., maximum $\Delta {\rm RV}_{\rm orb}$) at the RV measurement epoch. We therefore conservatively assume an uncertainty of 1.3 km s^{-1} on the system velocity as measured by the integrated-light RV.[15]

[14] We note that our estimate of RV systematic errors neglects the fact that slit losses can cause a binary to experience RV shifts depending on how the slit is centered with respect to the individual components. However, this approximation is justified here because the 0.″5 slit used by Shkolnik et al. and typical seeing values are ≳10× larger than the binary separation.

[15] We note that as a β Pic moving group member we would expect somewhat smaller integrated-light RV excursions for 2MASS J0249−0557AB than estimated above because a younger age corresponds to lower masses for the components of 2MASS J0249−0557AB and thereby a longer orbital period for a given semimajor axis. As we derive in Section 3.6, a smaller system mass of ≈0.1 $M_\odot$ is predicted from models, implying a longer orbital period of 8 years and thereby smaller median RV deviations of 0.10 km s^{-1} (up to 1.0 km s^{-1}) for an eccentric orbit. However, a change in RV uncertainty from 1.3 to 1.0 km s^{-1} has a negligible impact on our following analysis.

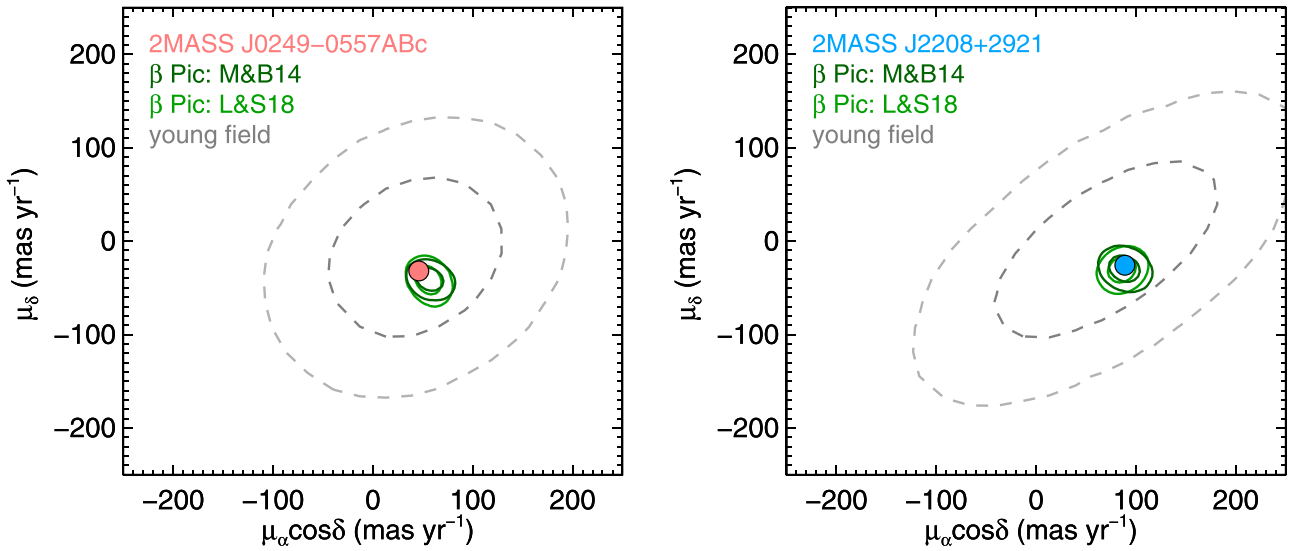

Figure 8. Measured proper motions for the 2MASS J0249−0557 system (left) and 2MASS J2208+2921 (right) shown alongside various populations that we simulated in *UVW* space and then projected into proper motion space using the measured parallaxes. Two different velocity ellipsoids are shown for the β Pic moving group from Mamajek & Bell (2014) and Lee & Song (2018), which give very similar results. The young field population is from the Besançon model of the Galaxy (Robin et al. 2003). For these populations of simulated objects, we show 2D contours containing 68.3% and 95.4% of the objects in proper motion space. The measured proper motions of both systems are consistent with β Pic membership but also with the broadly distributed young field population. (This is for display purposes only as our analysis is based on the full 3D kinematics including RV.)

3.3.2. Reaffirming ACRONYM Membership

Combining the RV from the Shkolnik et al. (2017) ACRONYM survey with our absolute parallax and proper motion, we find $(U, V, W) = (-10.7 \pm 0.9, -12.8 \pm 1.4, -9.8 \pm 1.1)$ km s^{-1} and $(X, Y, Z) = (-28 \pm 3, -0.68 \pm 0.07, -40 \pm 4)$ pc. Despite our parallax distance ($48.9^{+4.4}_{-5.4}$ pc) being somewhat smaller than the kinematic distance of 60 pc used in the analysis of Shkolnik et al., our *XYZ* values agree within 0.7–1.0σ of their values $(X, Y, Z) = (-35 \pm 4, -0.80 \pm 0.08, -49 \pm 5)$ pc. Here we assume that the *XYZ* uncertainties of Shkolnik et al. are dominated by kinematic distance uncertainty, which we estimate to be 10% based on the fractional error in the proper motion they used: $(44.6 \pm 4.1, -35.0 \pm 4.1)$ mas yr^{-1}. Compared to their $(U, V, W) = (-10.6, -16.2, -10.0)$ km s^{-1}, only the V component is more than 0.2σ different from our own measurements. Examining the covariance between our input measurements and output velocities indicates that this discrepancy in V is almost entirely due to the difference in the decl. component of our CFHT proper motion $\mu_\delta = -32.0 \pm 2.1$ mas yr^{-1} for 2MASS J0249−0557 c compared to -35.0 ± 4.1 mas yr^{-1} for 2MASS J0249−0557AB in Shkolnik et al. (2017). These two independent measurements are consistent within 0.7σ; therefore, we conclude that our updated *UVW* velocity is consistent within the 1σ uncertainties of the kinematic data used by Shkolnik et al. (2017). By extension, we expect that their assessment of 2MASS J0249−0557 as a likely member of the β Pic moving group would remain unchanged using our new proper motion, but we now consider membership in more detail given our addition of a parallax.

Because the β Pic moving group is spread over thousands of square degrees, both the directly observable kinematics of members (proper motion and RV) and contamination due to the field population will vary widely over the sky. Achieving a highly complete group census requires casting a wide net in kinematic space, but not so wide as to become unacceptably contaminated by field objects. We consider these two competing effects in the following.

First, to estimate the completeness of selecting β Pic group members using various kinematic criteria, we created a Monte Carlo population of simulated members at the sky position and distance of 2MASS J0249−0557. For the kinematics of the β Pic moving group, we consider two velocity ellipsoids derived from slightly different membership lists. One is the Gaussian ellipsoid derived by Mamajek & Bell (2014), which has a mean velocity of $(U, V, W) = (-10.9, -16.0, -9.2)$ km s^{-1} and intrinsic velocity dispersions along these axes of (1.5, 1.4, 1.8) km s^{-1}, respectively. This is based on the classic membership list of 26 stars from Zuckerman & Song (2004) plus four additional high-probability members from Malo et al. (2013). We also consider an ellipsoid based on a somewhat larger membership list of 57 stars from Lee & Song (2018) that was derived from a uniform assessment of all potential β Pic candidates in the literature at the time, selecting only the highest-probability members. The mean velocity of the Lee & Song (2018) ellipsoid, $(U, V, W) = (-10.5, -15.9, -9.1)$ km s^{-1}, is nearly identical to that of Mamajek & Bell (2014) but with dispersion axes that are rotated to match the covariances in the data as fit by three Euler angles. Our *UVW* for 2MASS J0249−0557AB places it 3.5 km s^{-1} away from the mean velocity of the β Pic moving group using either the Mamajek & Bell (2014) or Lee & Song (2018) results.

To properly account for all covariances, we project the *UVW* velocities of the simulated β Pic population into proper motions and RVs using the sky coordinates, parallax, and corresponding measurement uncertainties of the 2MASS J0249−0557 system. In proper motion–RV space, we can more clearly investigate observational selection effects. Figure 8 shows the projection of the 3D velocity ellipsoids into 2D proper motion space. For display purposes, Figure 8 also shows contours corresponding to the young field population (<150 Myr) as simulated in the Besançon model of the Galaxy (Robin et al. 2003). As expected, the field population spans a

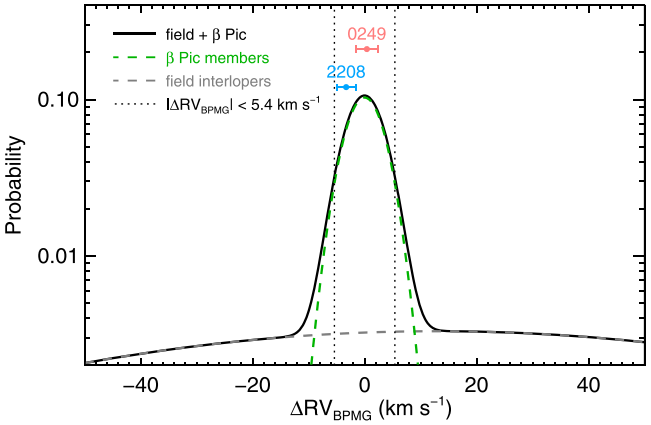

Figure 9. Probability distributions of ΔRV_{BPMG}, defined as the difference between an object's measured RV and the expected RV if it were a member of the β Pic moving group. The Gaussian distributions shown here were derived from all objects that passed proper motion and HR diagram selection criteria for membership in the β Pic moving group in the ACRONYM candidate sample (Shkolnik et al. 2017). After this sample was subjected to spectroscopic follow-up, 38% of objects were determined to be field interlopers lacking evidence of youth (Hα, Li I) or having RVs inconsistent with β Pic kinematics, and 62% were confirmed as likely members. The interlopers have widely varying RVs, while by definition the members are concentrated near ΔRV_{BPMG} of zero. Integrating the field interloper distribution over a range of ΔRV_{BPMG} then dividing by the integral of the combined distribution (field + β Pic) over the same ΔRV_{BPMG} range gives the field contamination rate. The original ACRONYM selection criterion of $|\Delta RV_{BPMG}| < 5.4$ km s^{-1} gives a 4% contamination rate. Horizontal error bars are plotted at arbitrary probability to show the ΔRV_{BPMG} values for 2MASS J0249−0557 and 2MASS J2208 +2921, where the error includes both the intrinsic dispersion in the β Pic group *UVW* ellipsoid and the RV measurement uncertainties.

large amount of parameter space, encompassing the entirety of the β Pic moving group and 2MASS J0249−0557.

For every simulated β Pic group member and 2MASS J0249 −0557 itself, we compute the 3D distance in ($\mu_\alpha \cos\delta$, μ_δ, RV) space from the mean velocity. In general, we quote 3D distances in units of σ, that is, normalized along each principal component axis by the standard deviation in that direction (a.k.a., the Mahalanobis distance). In 3D space, the usual Gaussian confidence intervals do not correspond to integer units of σ, but rather 68.3% of the distribution is contained within 1.88σ, 95.4% within 2.83σ, and so on. 2MASS J0249−0557 is fairly close to the mean velocity of the β Pic moving group, only 1.46σ and 1.32σ away from the ellipsoids of Mamajek & Bell (2014) and Lee & Song (2018), respectively. Among simulated β Pic group members, most of them (54% and 63%, respectively) are more distant than 2MASS J0249−0557 from the ellipsoid means. Thus, 2MASS J0249−0557 would pass any reasonably inclusive kinematic criteria for membership in the β Pic moving group using this approach.

To estimate the probability that 2MASS J0249−0557 could be a field interloper that happens to share the kinematics of the β Pic moving group, we consider the ACRONYM search in which it was originally identified (Shkolnik et al. 2017). The first step in this search was to select candidates based on astrometry and photometry, using proper motions to estimate a kinematic distance (the distance required to minimize the difference between the measured and expected proper motion of a β Pic member at the given R.A. and decl.) and spectral energy distributions (SEDs) to estimate spectral types. Of the 4.5×10^3 objects with proper motions consistent with β Pic kinematics, only 104 objects with estimated spectral types of K7–M9 were consistent with being young on the H-R diagram and thus selected for spectroscopic follow-up. The latest-type sources were first screened for signs of low gravity using low-resolution IR spectra. High-resolution optical spectroscopy was obtained for all remaining objects to measure RVs and look for Hα emission and Li I absorption. This resulted in 91 objects with RV measurements, including both β Pic members and field contaminants. For each object, Shkolnik et al. (2017) computed the expected RV for β Pic motion, and the difference from the measured value (ΔRV_{BPMG}) was used, along with other youth indicators, in assigning final memberships. Here we use the ΔRV_{BPMG} distribution of the objects that Shkolnik et al. (2017) classified as nonmembers to estimate the fraction of field interlopers that would pass both the initial proper motion and final RV selection.

We assume that both populations (members and nonmembers) found in the ACRONYM search can be approximated as Gaussians in ΔRV_{BPMG}. The nonmembers should be distributed widely in ΔRV_{BPMG} while members cluster tightly around zero. Shkolnik et al. (2017) used a threshold in ΔRV_{BPMG} of 5.4 km s^{-1} to select members, corresponding to a 3σ cut given the velocity dispersion of 1.8 km s^{-1} used in their analysis for the β Pic moving group. We assume that the subset of 32 objects that did not pass their ΔRV_{BPMG} cut or lacked Hα emission (as expected at the age of β Pic) represent the contaminant population, and these objects have a mean and standard deviation in ΔRV_{BPMG} of 13 ± 46 km s^{-1}. In contrast, the 52 objects identified as members have a ΔRV_{BPMG} mean and standard deviation of 0.3 ± 2.4 km s^{-1}. (Here we have excluded seven objects with ambiguous status, mostly spectroscopic binaries where the RV likely has a systematic orbital offset.) To compute a false alarm rate, we combine these two Gaussians into a single probability distribution, normalized according to $52/84 = 62\%$ members (centered at $\Delta RV_{BPMG} = 0$) and $32/84 = 38\%$ contaminants.

For a given ΔRV_{BPMG} selection criterion, the false-alarm rate is the integral of the nonmember distribution divided by the integral of the combined distribution over the same ΔRV_{BPMG} range (Figure 9). Using the original ACRONYM criterion of $|\Delta RV_{BPMG}| < 5.4$ km s^{-1}, we compute a false-alarm rate of 4%. Even if we consider an extremely restrictive criterion of $|\Delta RV_{BPMG}| < 0.8$ km s^{-1}, which would let past just 2MASS J0249−0557 and 11 other members, the false-alarm rate would only be reduced to 3.1%. Therefore, contamination does not strongly depend on the ΔRV_{BPMG} cut, as long as the cut is relatively restrictive.

According to the binomial distribution, a false alarm rate of 4% implies a 90% probability of at least one contaminant among the 52 objects that Shkolnik et al. (2017) identified as members meeting this criterion and a <1% probability of $\geqslant$7 contaminants. However, the appropriate sample to consider here is the set of 12 latest-type ACRONYM members accessible from CFHT that we have been following up to obtain parallaxes. Among all 12, only 0.5 contaminants are expected for a 4% false alarm rate, and $\leqslant$3 should be present at 99% confidence. 2MASS J0249−0557 is the first object for which we are reporting a parallax, so it is not yet possible to determine if the parallaxes and improved proper motions for the other objects are consistent with β Pic membership or not.

The false alarm rate of 4% derived for the ACRONYM sample should be considered a conservative upper limit in the case of 2MASS J0249−0557. First, parallaxes were not available in the ACRONYM sample selection. If they were,

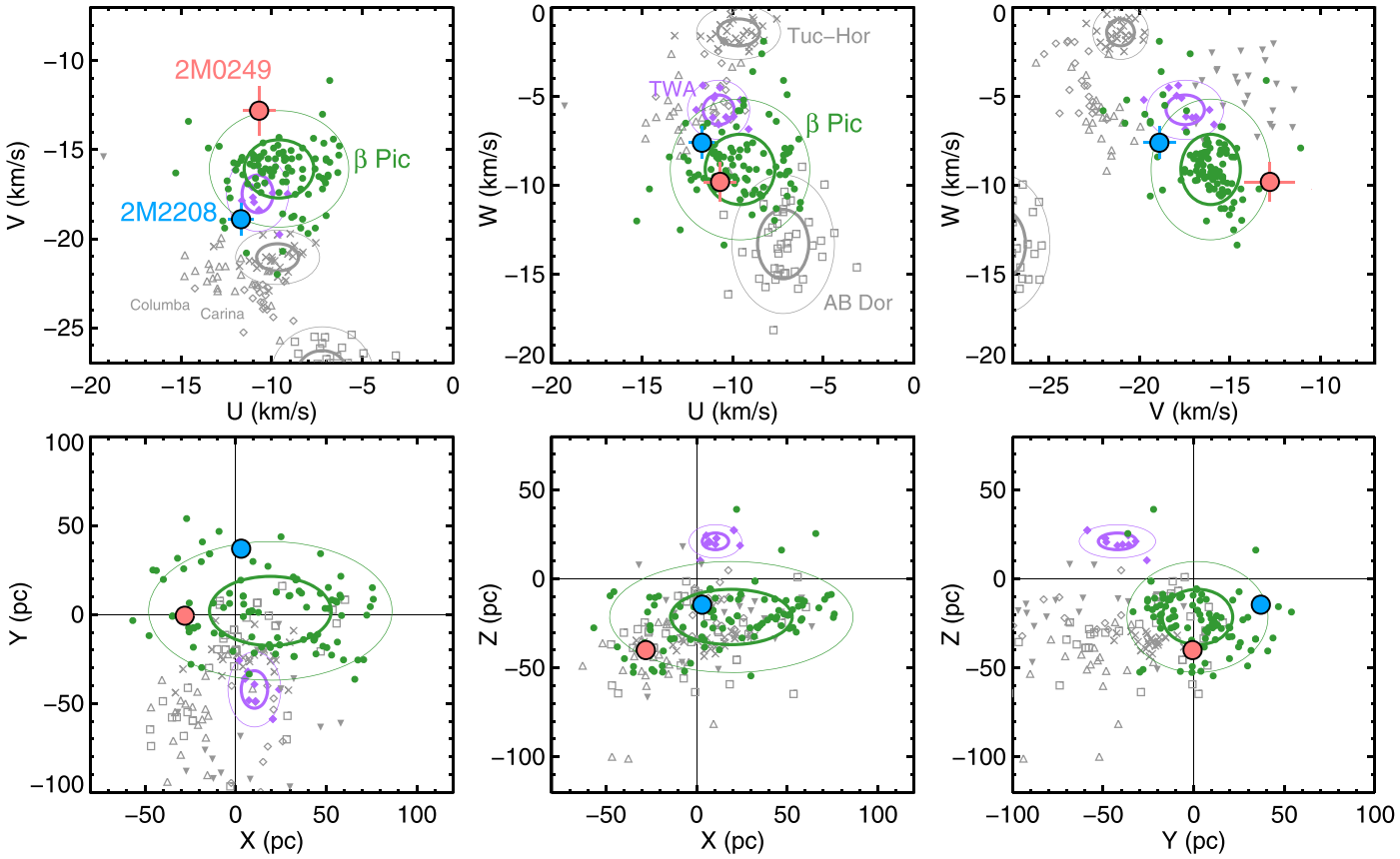

Figure 10. Kinematic (*UVW*) and spatial (*XYZ*) position of the 2MASS J0249−0557 system and 2MASS J2208+2921 compared to known young moving groups. The β Pic and TWA groups are highlighted in color, as the two nearest groups in *UVW*, but only β Pic also agrees in *XYZ*. The group members plotted here are from Torres et al. (2008), and for β Pic we also include objects from Shkolnik et al. (2017). Ellipses represent the 1σ and 2σ bounds of members plotted here, and these are also shown for the Tuc-Hor and AB Dor groups in *UVW* given their large sample sizes, though they do not match well with 2MASS J0249−0557. This plot is for display purposes only. Our kinematic analysis uses *UVW* ellipsoids defined by the much more restrictive, but spatially incomplete, lists of high-probability members compiled by Mamajek & Bell (2014) and Lee & Song (2018).

then they would have reduced the number of interlopers that made it to the spectroscopic follow-up stage of the ACRONYM search and thereby reduced the nonmember component of the probability distribution used above. Our addition of a parallax for 2MASS J0249−0557 could have ruled out membership by being inconsistent with the β Pic group kinematic distance, but it did not. Second, spectroscopic binaries that are true members may have been excluded from the ACRONYM member sample due to orbital RV deviations. If such objects had not been excluded, that would have increased the relative number of members to nonmembers adopted in our analysis. Third, we used both young and old stars in our analysis to improve statistics and because stars from ACRONYM do not have homogeneous constraints on their ages. The detection of Li I absorption in 2MASS J0249−0557 provides a much stronger constraint than Hα in an earlier-type ACRONYM star lying above the lithium-depletion boundary. To determine an age constraint for 2MASS J0249−0557, we examined other associations with measured lithium-depletion boundaries. The components of 2MASS J0249−0557AB have bolometric magnitudes of $M_{\rm bol} = 11.21^{+0.24}_{-0.22}$ mag and $11.33^{+0.24}_{-0.22}$ mag (Section 3.2) that are both consistent within their errors with the boundary of $M_{\rm bol} = 11.31$ mag for α Persei (85 ± 10 Myr; Barrado y Navascués et al. 2004), implying a system age $\lesssim$100 Myr. This is somewhat stronger than the age constraint implied by the gravity classifications of VL-G for both 2MASS J0249−0557AB and 2MASS J0249−0557 c ($\lesssim$150 Myr; e.g., Liu et al. 2016). If we were able to restrict the field interloper population used in our false-alarm analysis to such young stars, the false-alarm probability of 4% would be reduced by a factor roughly equal to the number of >100 Myr old stars divided by the number of <100 Myr old stars, which is likely at least an order of magnitude.

We conclude that the 2MASS J0249−0557 system is a very likely member of the β Pic moving group given its excellent kinematic agreement, low false-alarm probability, and independent constraints on youth (lithium and low-gravity classification) that are consistent with the age of the group. Although we have chosen not to use the spatial *XYZ* position of 2MASS J0249−0557 in our membership probability analysis, because the current census of the β Pic moving group has not been established to be complete, 2MASS J0249−0557 seems to be well within the spatial range of other β Pic members (Figure 10). It is also within the minimum volume enclosing ellipsoid of the "exclusive" (smallest) list of members shown in Figure 4 of Lee & Song (2018).

3.3.3. Comparison to Membership Tools

Generalized tools are available in the literature that provide young moving group membership probability estimates given

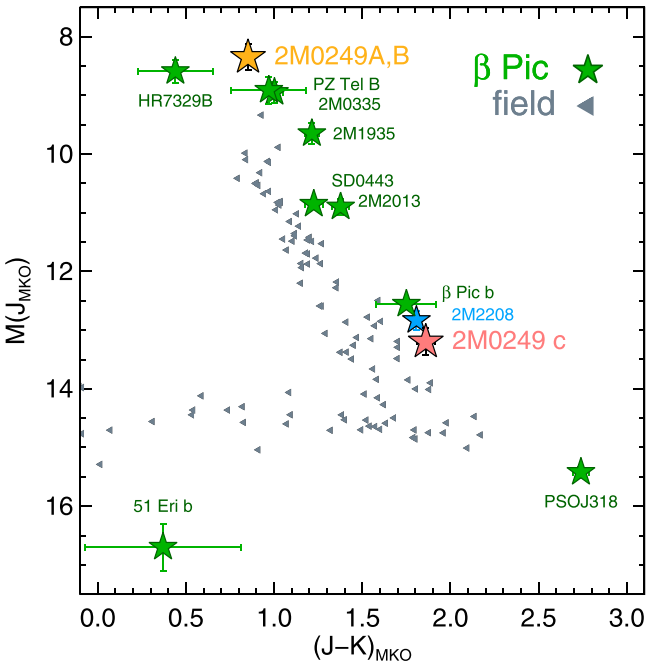

Figure 11. Color–magnitude diagram showing the 2MASS J0249−0557 system, the possible member 2MASS J2208+2921, other ultracool members of the β Pic moving group with parallaxes, and field ultracool dwarfs. Our new companion 2MASS J0249−0557 c (L2 VL-G) lies in a similar part of the diagram as the planet β Pic b (L2) and the free-floating object 2MASS J2208 +2921 (L3 VL-G). The components of 2MASS J0249−0557AB (M6 VL-G) have colors and magnitudes similar to the companions HR 7329B (M7.5) and PZ Tel B (M7), as well as the free-floating object 2MASSJ 0335+2342 (M7 VL-G). For 2MASS J0249−0557AB, we show the integrated-light photometry divided by two, assuming equal fluxes and colors. (Field dwarfs are from the Database of Ultracool Parallaxes at http://www.as.utexas.edu/~tdupuy/plx/; Dupuy & Liu 2012.)

input data (R.A., decl., proper motion, parallax, and RV). We have examined membership assessments from these tools as a point of comparison to our own membership analysis that is tailored to the case of 2MASS J0249−0557 and accounts for the particular selection process of the ACRONYM search. The underlying assumptions used in each tool varies, such as the number of associations included and their properties, so they can produce wide-ranging results for the same input data. We discuss the results from some commonly used tools before examining in detail the results of the current version of BANYAN.

The convergent point tool[16] from Rodriguez et al. (2013) takes only R.A., decl., and proper motion as inputs, and it outputs >10% probabilities for all seven populations it considers. The highest probability is 89% for the β Pic moving group, and the next highest is 57% for Columba. This convergent point tool also outputs a kinematic distance and RV for each group, and the value that is closest to the system RV of 2MASS J0249−0557 is the one for the β Pic moving group (13.4 km s^{-1}). The kinematic distance of 60 pc for β Pic membership is also consistent within the uncertainties of our parallactic distance. BANYAN I[17] uses a Bayesian approach to assign an input object to one of seven groups or the field population (Malo et al. 2013). From the proper motion, parallax, and RV of 2MASS J0249−0557, it computes membership probabilities of 92% for the β Pic moving group and 8% for the field. The convergence-style algorithm LACEwING[18] (Riedel et al. 2017) considers 16 associations, and while the highest output probability is for the β Pic moving group, it is only 3%. None of these tools can incorporate additional information, such as the age constraint on 2MASS J0249−0557 of <100 Myr, but they are generally consistent with β Pic moving group membership.

BANYAN Σ is the latest version of perhaps the most widely used membership tool, and it includes 27 young associations and the field population (Gagné et al. 2018). It is different from previous versions of BANYAN (e.g., Gagné et al. 2014) in that it is designed to deliver a uniform 90% true positive rate for all groups when providing a proper motion, parallax, and RV and selecting objects above a threshold output probability of >90%. Using v1.1 of the BANYAN Σ tool (Gagné 2018) and including both *UVW* and *XYZ* for 2MASS J0249−0557 in the analysis, BANYAN Σ reports probabilities of 11% for the β Pic moving group, 89% for the field population, and negligible probabilities for other groups. Neither probability crosses the 90% threshold, and although the β Pic probability is low, it is not necessarily discrepant with our analysis showing that 2MASS J0249−0557 is a likely β Pic member. This is primarily because BANYAN Σ does not account for additional information about youth, such as the detection of lithium in 2MASS J0249−0557AB, which should greatly reduce the prior likelihood that the system is a field interloper.

To try to estimate the field prior used by BANYAN Σ at the location of 2MASS J0249−0557, we excluded kinematic information (set proper motion and RV errors to arbitrarily large values) and retained spatial information (R.A., decl., and parallax). This gave a field probability of 94.8% and Tuc-Hor probability of 4.1%, followed by AB Dor (0.5%), Columba (0.3%), and β Pic (0.3%). The Tuc-Hor probability is strikingly high given the location of 2MASS J0249−0557 at $(X, Y, Z) = (-28 \pm 3,\ -0.68 \pm 0.07,\ -40 \pm 4)$ pc, a region of space mostly devoid of known Tuc-Hor members (e.g., see Figure 10 of Kraus et al. 2014). This apparent discrepancy is likely a consequence of the specialized way that BANYAN Σ determines its priors for young moving groups relative to the field. Normalization factors denoted as $\ln(\alpha_k)$ are chosen to ensure a 90% true positive rate for all groups, regardless of their spatial or kinematic concentration. This makes it difficult to quantify the field prior relative to the β Pic moving group prior and how that would change when considering only young field interlopers. Therefore, we instead consider the true-positive and false-positive rates reported by BANYAN Σ.

In BANYAN Σ, the field probability should not be interpreted as an estimate of the false-positive rate. For example, a hypothetical object with proper motion, parallax, and RV giving a 90% probability of belonging to the β Pic moving group and a 10% field probability has a 90% true-positive rate (by design) and a very low false-positive rate of 1.6×10^{-5} (Table 9 of Gagné et al. 2018). This is consistent with the intention of BANYAN Σ to be readily used on large input data sets, where even such a low rate could result in hundreds of contaminants. However, a true-positive rate of 90% corresponds to a false-negative rate of 10%, which is rather conservative (i.e., equivalent to a 1.6σ selection criterion). Adopting such a criterion would have the undesirable effect that any of the 12 objects in our ACRONYM

[16] http://dr-rodriguez.github.io/CPCalc.html
[17] http://www.astro.umontreal.ca/~malo/banyan.php
[18] https://github.com/ariedel/lacewing

parallax follow-up sample would more likely be rejected as a false negative (10%) than accepted as a false positive ($\leqslant$4%, according to our ACRONYM-based analysis in the previous section). To reduce the false-negative rate, we consider a BANYAN Σ β Pic moving group probability of 10% (comparable to 11% for 2MASS J0249−0557), for which the true-positive rate is 95.57% (i.e., equivalent to a 2.0σ selection criterion), and the false-positive rate is still only 2.0×10^{-4} (J. Gagné 2018, private communication). We suggest that such a more-inclusive member selection would be reasonable for a small sample like our parallax follow-up of 12 ultracool dwarfs from ACRONYM.

To summarize, each of the generalized membership tools we examined gives a higher membership probability for the β Pic moving group than any other young association. The output probabilities vary widely, and they should be considered lower limits because none of these tools can account for the prior age information that 2MASS J0249−0557 is young ($\lesssim$100 Myr from lithium depletion and spectrally classified as low gravity). The false-positive rate predicted by BANYAN Σ for 2MASS J0249−0557 is much lower than the conservative upper limit we derived for the entire ACRONYM sample in the previous section ($\leqslant$4%). Overall, examination of these membership tools supports the conclusion from our independent analysis, based on modeling the selection effects of the ACRONYM sample and our CFHT parallax follow-up, that the 2MASS J0249−0557 system is a β Pic moving group member.

3.4. Membership Assessment for 2MASS J2208+2921

In our previous work, Liu et al. (2016) identified the L3 VL-G dwarf 2MASS J2208+2921 as a promising candidate member of the β Pic moving group based on our parallax and proper motion but in need of RV confirmation. Since then, Vos et al. (2017) measured an RV of $-15.7^{+0.8}_{-0.9}$ km s^{-1}. Combining all these measurements gives $(U, V, W) = (-11.7 \pm 0.7, -18.9 \pm 0.9, -7.6 \pm 0.9)$ km s^{-1}, which is 3.6 km s^{-1} away from the mean β Pic group velocity of Mamajek & Bell (2014) and 3.8 km s^{-1} away from the mean velocity of Lee & Song (2018). Projecting the β Pic ellipsoids into proper motion–RV space, as in our analysis of 2MASS J0249−0557 in the previous section, we find 3D distances for 2MASS J2208+2921 that are 2.0σ using the Mamajek & Bell (2014) group parameters and 2.2σ using Lee & Song (2018). (Even though 2MASS J2208+2921 has similar distances in km s^{-1} from the β Pic ellipsoids as 2MASS J0249−0557, it has slightly larger 3D distances in σ because its parallax, proper motion, and RV are more precise.) The fraction of simulated β Pic members that are closer than 2MASS J2208+2921 in 3D space are 73% and 82%, respectively. Thus, even a >90% completeness criterion would require 2MASS J2208+2921 to be considered a candidate member. Unlike 2MASS J0249−0557, most of the 3D distance is in the RV axis, but with $\Delta RV_{BPMG} = -3.3 \pm 1.7$ km s^{-1}, 2MASS J2208+2921 is still within <2σ of the expected velocity for a member and would easily pass the RV criterion used for the ACRONYM sample (Figure 9).Therefore, based on kinematics alone, 2MASS J2208+2921 appears to be a likely member of the β Pic moving group.

Spatially, 2MASS J2208+2921 coincides with other published members of the β Pic moving group given its position of $(X, Y, Z) = (3.1 \pm 0.2, 37.0 \pm 2.4, -14.5 \pm 0.9)$ pc (Figure 10). Compared only to stars belonging to the most restrictive member lists, it is somewhat discrepant in the Y axis; for example, it lies just outside the minimum volume enclosing ellipsoid of Lee & Song (2018). This may not be a major cause for concern, as it has been suggested that the spatial distribution of members may be larger than is currently known, especially for widely dispersed groups like β Pic and AB Dor (e.g., Liu et al. 2016; Bowler et al. 2017; Desrochers et al. 2018).

BANYAN Σ reports a surprisingly low probability of 0.8% for β Pic membership (99.2% for field) for 2MASS J2208+2921. This in contrast with the previous β Pic probability of 18% computed by Liu et al. (2016) using BANYAN II (Gagné et al. 2014) with the same proper motion and parallax, as well as a membership probability of 96.5% using BANYAN I (Malo et al. 2013) with both a parallax and RV. The only change in the observations since Liu et al. (2016) is the addition of an RV from Vos et al. (2017), which is consistent with the expected value for β Pic within 2σ even according to BANYAN Σ (optimal RV of -13.6 ± 0.7 km s^{-1}). As for other membership tools, they also give a higher membership probability for the β Pic moving group than any other young association, with 94% from the convergent point tool (Rodriguez et al. 2013) and 19% from LACEwING (Riedel et al. 2017).

The discrepancy between 2MASS J2208+2921 passing the same kinematic selection criteria as 2MASS J0249−0557 and the >10× lower membership probability from BANYAN Σ may be related to the fact that BANYAN Σ does not account for evidence of youth that would reduce the fraction of field interlopers. Given the VL-G gravity classification, 2MASS J2208+2921 is quite young. Among parallax-confirmed members of young moving groups, Liu et al. (2016) found that the VL-G classification becomes less prevalent by an age of ≈150 Myr compared to the intermediate-gravity classification INT-G. This trend is less clear among (less definitive) candidate lists for moving groups using objects that lack parallaxes or RVs (e.g., Gagné et al. 2015c; Faherty et al. 2016). Still, all previously known parallax- and RV-confirmed ultracool dwarf members of the β Pic moving group are classified as VL-G. Therefore, 2MASS J2208+2921 is independently known to be consistent with the age of the β Pic group, which reduces the probability that it is a field interloper.

We conclude that 2MASS J2208+2921 is a possible member of the β Pic moving group, but given the discord with BANYAN Σ, we consider its status ambiguous. Unlike 2MASS J0249−0557, there is little room for improving the observations of 2MASS J2208+2921 (system RV, distance, proper motion), so a more robust look at its membership will need a more complete census of β Pic members. *Gaia* will not map the spatial distribution of young L dwarfs out to the necessary distances for such work, due to their faintness (e.g., 2MASS J2208+2921 itself does not have an entry in *Gaia* DR2). However, it should be possible to use the higher mass M dwarfs to better determine the spatial distribution of the β Pic moving group.

3.5. Color–Magnitude Diagram

Combining our photometry with the distance modulus derived from our parallax ($m - M = 3.44^{+0.21}_{-0.23}$ mag) allows us to compute absolute magnitudes and compare them to the polynomial relations of magnitude versus spectral type from Liu et al. (2016). For a spectral type of L2 ± 1 VL-G, the polynomials give

Table 5
Late-type Members of the β Pic Moving Group

Name	Spectral Type	π (mas)	$m_{\rm bol}$ (mag)	log ($L_{\rm bol}/L_\odot$) (dex)	Mass ($M_{\rm Jup}$)	References
PZ Tel B	M7	19.4 ± 1.0	14.44 ± 0.15	−2.45 ± 0.07	61 ± 12	F15, M16, v07
2MASSI J0335020+234235	M7 VL-G	21.8 ± 1.8	14.29 ± 0.05	−2.50 ± 0.08	56^{+13}_{-12}	AL13, D18, L16, S17
HR 7329B	M7.5	20.74 ± 0.21	14.60 ± 0.16	−2.58 ± 0.07	49^{+12}_{-10}	L00, v07, F15
2MASS J0249−0557A	M6 VL-G	20.5 ± 2.1	14.65 ± 0.05	−2.59 ± 0.09	48^{+13}_{-12}	D18
2MASS J0249−0557B	M6 VL-G	20.5 ± 2.1	14.77 ± 0.05	−2.64 ± 0.09	44^{+14}_{-11}	D18
SDSS J044337.60+000205.2	L0 VL-G	47.3 ± 1.0	14.43 ± 0.06	−3.23 ± 0.03	20^{+4}_{-5}	AL13, D18, L16, RB09
β Pic b	L2[a]	51.44 ± 0.12	15.63 ± 0.08	−3.78 ± 0.03	$13.0^{+0.4}_{-0.3}$	D18, v07, M15
2MASS J0249−0557 c	L2 VL-G	20.5 ± 2.1	18.18 ± 0.06	−4.00 ± 0.09	$11.6^{+1.3}_{-1.0}$	D18
PSO J318.5338−22.8603	L7 VL-G	45.1 ± 1.7	17.85 ± 0.12	−4.55 ± 0.06	$6.5^{+1.2}_{-0.8}$	D18, L13, L16, A16
51 Eri b	T6.5 ± 1.5	33.98 ± 0.34	21.8 ± 0.4	−5.87 ± 0.15	2–12[b]	R17, v07
Possible Members (π or RV unavailable, or ambiguous membership)						
2MASS J02241739+2031513	M6 INT-G	⋯	⋯	⋯	⋯	S17
2MASS J03363144−2619578	M6 VL-G	⋯	⋯	⋯	⋯	S17
2MASS J03370343−3042318	M6 FLD-G	⋯	⋯	⋯	⋯	S17
2MASS J19082195−1603249	M6 VL-G	⋯	⋯	⋯	⋯	S17
2MASS J23355015−3401477	M6 VL-G	⋯	⋯	⋯	⋯	S17
2MASS J22334687−2950101	M7 VL-G	⋯	⋯	⋯	⋯	S17
2MASS J23010610+4002360	M7 VL-G	⋯	⋯	⋯	⋯	S17
DENIS J004135.3−562112AB	M7.5 VL-G	⋯	⋯	⋯	⋯	G15
2MASS J03550477−1032415	M8 INT-G	⋯	⋯	⋯	⋯	S17
2MASS J19355595−2846343	M9 VL-G	14.2 ± 1.2	15.9 ± 0.2	−2.76 ± 0.11	35^{+7}_{-15}	AL13, D18, L16
2MASS J20004841−7523070	M9 VL-G	⋯	⋯	⋯	⋯	G15
2MASS J00464841+0715177[c]	L0 VL-G	⋯	⋯	⋯	⋯	G15, F16
2MASS J20135152−2806020	L0 VL-G	21.0 ± 1.3	16.18 ± 0.05	−3.22 ± 0.06	20^{+4}_{-6}	AL13, D18, L16
EROS-MP J0032−4405[d]	L0 INT-G	⋯	⋯	⋯	⋯	AL13, G14, G15b
2MASSW J2208136+292121[e]	L3 VL-G	25.1 ± 1.6	17.41 ± 0.08	−3.87 ± 0.07	$12.6^{+0.7}_{-0.5}$	AL13, D18, L16, V17
Candidates (proper motion only)						
2MASS J20334670−3733443	M6 INT-G	⋯	⋯	⋯	⋯	G15
2MASS J01294256−0823580	M7 VL-G	⋯	⋯	⋯	⋯	G15
2MASS J02501167−0151295	M7 VL-G	⋯	⋯	⋯	⋯	G15
2MASS J05120636−2949540	L5 INT-G	⋯	⋯	⋯	⋯	G15
2MASS J23542220−0811289	L5 VL-G	⋯	⋯	⋯	⋯	Sc17
2MASS J00440332+0228112	L7 VL-G	⋯	⋯	⋯	⋯	Sc17

Notes. This table does not include nine new candidates identified by Gagné & Faherty (2018) using parallaxes and proper motions from the *Gaia* DR2 catalog because the objects have not been spectroscopically confirmed (photometrically estimated spectral types of M6–L3).
[a] Spectral resolution insufficient for gravity classification.
[b] The luminosity of 51 Eri b is low enough to be consistent with both hot-start and cold-start models, so its mass is correspondingly very uncertain.
[c] Gagné et al. (2015c) reported this as a β Pic moving group candidate, but Faherty et al. (2016) classify it as an ambiguous member after measuring an RV.
[d] There are two published parallaxes for EROS-MP J0032−4405. The value of 38.4 ± 4.8 mas from Faherty et al. (2012) used to determine β Pic membership by Gagné et al. (2014, 2015c) is 1.8× larger than the value of 21.6 ± 7.2 mas from Marocco et al. (2013) used by Faherty et al. (2016) to determine high-likelihood AB Dor membership.
[e] Our kinematic analysis indicates likely membership for 2MASS J2208+2921 based on proper motion, parallax, and RV. But this is discordant with the results of BANYAN Σ, so we consider the membership status ambiguous.
References. (A16) Allers et al. (2016), (AL13) Allers & Liu (2013), (D18) this work, (F15) Filippazzo et al. (2015), (F16) Faherty et al. (2016), (G14) Gagné et al. (2014), (G15) Gagné et al. (2015c), (G15b) Gagné et al. (2015b), (L00) Lowrance et al. (2000), (L13) Liu et al. (2013), (L16) Liu et al. (2016), (M15) Morzinski et al. (2015), (M16) Maire et al. (2016), (R17) Rajan et al. (2017), (RB09) Reiners & Basri (2009), (S17) Shkolnik et al. (2017), (Sc17) Schneider et al. (2017), (v07) van Leeuwen (2007), (V17) Vos et al. (2017).

$M_J = 12.4 \pm 1.0$ mag and $M_K = 10.6 \pm 0.9$ mag, where the uncertainties are a quadrature sum of the rms of objects used in the fit about the polynomial curve (±0.6 mag and ±0.4 mag, respectively) and the propagation of the spectral type uncertainty (±0.8 mag). The absolute magnitudes of 2MASS J0249−0557 c are $M_J = 13.20^{+0.22}_{-0.24}$ mag and $M_K = 11.34^{+0.22}_{-0.24}$ mag, which are 0.8σ and 0.9σ fainter than the polynomial and thus consistent with being a normal object for its spectral type and gravity classification. Its faintness also suggests that 2MASS J0249−0557 c is not likely to be an unresolved, near-equal-flux binary. For the M6 VL-G integrated-light spectral type of 2MASS J0249−0557AB, the Liu et al. (2016) polynomial gives $M_K = 7.2 \pm 0.4$ mag. (The polynomial is only valid for types M6 and later, so we cannot reliably estimate the additional error due to a ±1 subtype uncertainty.) Our resolved K-band magnitudes of the primary ($M_K = 8.29^{+0.21}_{-0.23}$ mag) and secondary ($M_K = 8.41^{+0.21}_{-0.23}$ mag) are 1.1 mag and 1.2 mag fainter, respectively, than the polynomial but again not overly discrepant within the scatter about the

polynomials. For context, there are other examples of low-gravity M6 dwarfs with similar or fainter absolute magnitudes, such as HD 1160B ($M_K = 8.83 \pm 0.16$ mag; Nielsen et al. 2012).

Figure 11 shows the components of the 2MASS J0249−0557 triple system alongside members of the β Pic moving group on an IR color–magnitude diagram. 2MASS J0249−0557AB has a color similar to other late-M members of β Pic, like PZ Tel B (M7) and 2MASS J0335+2342 (M7 VL-G), and each component has a comparable or somewhat brighter absolute magnitude, if we assume the two components have similar infrared colors. Likewise, 2MASS J0249−0557 c lies near the other β Pic objects with L1–L3 spectral types: β Pic b and 2MASS J2208+2921.

3.6. Estimated Masses

In order to derive physical properties, we rely on the predicted luminosity ($L_{\rm bol}$) as a function of mass and age from evolutionary models. We compute luminosities by combining the bolometric fluxes derived in Section 3.2 with our parallax measurement of 20.5 ± 2.1 mas. For 2MASS J0249−0557 c, we find $\log(L_{\rm bol}/L_\odot) = -4.00 \pm 0.09$ dex. For 2MASS J0249−0557AB, we divide its integrated-light luminosity assuming that the nearly equal-flux components ($\Delta K = 0.123 \pm 0.005$ mag) have a negligible difference in their K-band bolometric corrections compared to the uncertainty in the distance modulus ($3.44^{+0.21}_{-0.23}$ mag). Thus, adopting our K-band flux ratio as the bolometric flux ratio results in component luminosities of $\log(L_{\rm bol}/L_\odot) = -2.59 \pm 0.09$ dex and -2.64 ± 0.09 dex.

No single model grid completely covers the luminosities of all three components, so we use the Baraffe et al. (2015) tracks for 2MASS J0249−0557AB and Saumon & Marley (2008) hybrid tracks for 2MASS J0249−0557 c. In a fashion similar to that of Dupuy & Liu (2017), we use Monte Carlo rejection sampling with uniformly distributed masses and ages as the initial input. For each trial mass and age, we compute

$$\chi^2 = \left(\frac{\log(L_{\rm bol,model}) - \log(L_{\rm bol})}{\sigma_{\log(L_{\rm bol})}}\right)^2 + \left(\frac{t - 22\ {\rm Myr}}{6\ {\rm Myr}}\right)^2,$$

from which we compute a rejection probability $p = e^{-(\chi^2 - \min(\chi^2))/2}$. We then draw random, uniformly distributed variates u and reject samples where $p < u$. This method allows us to properly account for the possibility that objects of different masses and ages have the same luminosity due to deuterium fusion, which can be important at such young ages. The age prior of 22 ± 6 Myr is based on the most recent measurement of the lithium-depletion boundary in the β Pic moving group from Shkolnik et al. (2017), which is consistent with the previous lithium-depletion age of 23 ± 3 Myr from Binks & Jeffries (2014) and the isochronal age of 24 ± 3 Myr from Bell et al. (2015).

Table 4 gives the resulting masses of the three components. As expected given its M6 VL-G spectral type, the tight binary 2MASS J0249−0557AB is estimated to be a pair of brown dwarfs, while the L2 VL-G companion's mass of $11.6^{+1.3}_{-1.0}$ $M_{\rm Jup}$ is likely below the deuterium fusion boundary (≈13 $M_{\rm Jup}$; e.g., Spiegel et al. 2011). For comparison, we also derived masses for other late-type members of β Pic using the Saumon & Marley (2008) models and the same rejection sampling method. For the free-floating objects, we computed our own

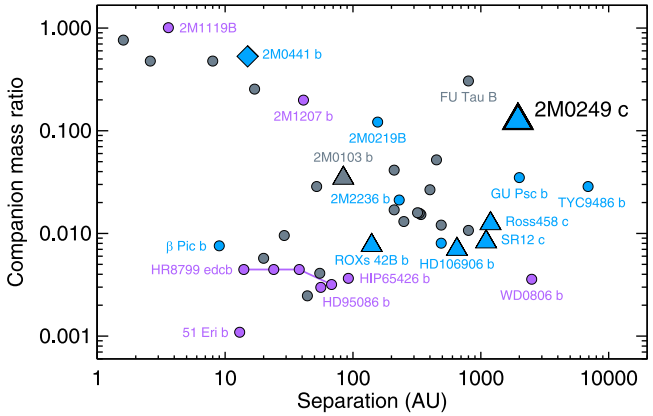

Figure 12. Companion mass ratio ($M_{\rm comp}/M_{\rm host}$) as a function of separation for directly imaged companions that have mass estimates near or below the deuterium-fusion limit (13 $M_{\rm Jup}$). Symbol shapes indicate companions to single stars (circles), binaries (triangles), or a member of a quadruple system (diamond). Symbol colors correspond to estimated masses from hot-start models: purple for the lowest-mass objects (⩽10 $M_{\rm Jup}$ even including 1σ uncertainties), blue for slightly higher mass objects (⩽15 $M_{\rm Jup}$ even including 1σ uncertainties), and gray for all other objects (>15 $M_{\rm Jup}$). 2MASS J0249−0557 c ($11.6^{+1.3}_{-1.0}$ $M_{\rm Jup}$) has an unusual combination of high mass ratio (∼0.1) and wide separation (1950 ± 200 au), strikingly different from the other planetary-mass companions in the β Pic moving group (β Pic b and 51 Eri b), which are among the smallest-separation, lowest-mass-ratio companions known. For this plot, we used the compilation of system properties from Bowler (2016) and added HIP 65426 b (Chauvin et al. 2017), 2MASS J2236+4751 b (Bowler et al. 2017), 2MASS J1119−1137AB (Best et al. 2017), and HD 203030B (Metchev & Hillenbrand 2006; Miles-Páez et al. 2017). When a companion orbits a binary, we use the total mass of the binary to compute the mass ratio. 2MASS J0249−0557 c would thus have a plotted mass ratio ≈2× higher if we used the primary component's mass (48^{+13}_{-12} $M_{\rm Jup}$) instead. (The blue circle without a label near HD 106906 b is HD 203030B.)

bolometric fluxes using the same method described in Section 3.2, except that in these cases we simply used published IRTF/SpeX spectra combined with BT-Settl models at other wavelengths. This included 2MASS J0335+2342, SDSS J0443+0002, 2MASS J1935−2846, 2MASS J2013−2806, PSO J318.5−22, and 2MASS J2208+2921. For companions, we used published values from the literature for β Pic b and 51 Eri b, and K_S-band photometry combined with the spectral type–BC$_{K_s}$ relation for young objects from Filippazzo et al. (2015) for PZ Tel B and HR 7329B. All of the luminosities and derived masses are given in Table 5. We emphasize that none of our quoted mass errors attempt to account for unknown systematic uncertainties in the evolutionary models, which are likely larger than the random errors in cases where luminosity is measured very precisely. We also note that formal mass errors are larger for the higher mass components 2MASS J0249−0557AB than for the wide companion 2MASS J0249−0557 c because the evolutionary models predict that such young, massive brown dwarfs have similar masses at a fixed age. In other words, isomass tracks pile up on an $L_{\rm bol}$–age diagram due to deuterium fusion; for example, see Figure 1 in Burrows et al. (2001).

3.7. Gaia DR2

A parallax and proper motion for 2MASS J0249−0557AB (in integrated light) are available from *Gaia* DR2 (Gaia Collaboration et al. 2016, 2018). Binary orbital motion can impact the parallax and proper motion in an unpredictable, systematic way, especially when there are relatively few independent observation epochs (DR2 reports `visibility_periods_used = 10` for this

system). Indeed, the excess source noise (ϵ_i) reported in DR2 for 2MASS J0249−0557AB is 0.70 mas at a significance of 37σ, suggesting that systematic, correlated noise from orbital motion impacts the five-parameter DR2 solution. There is evidence from hierarchical M dwarf triple systems, where one component is single and the other is unresolved in *Gaia* (e.g., GJ 1245 and GJ 2069), that parallax systematics for unresolved binaries can be up to at least 2 mas ($\approx 20\sigma$) with even larger proper motion systematics. Therefore, we have chosen not to use the DR2 astrometry for 2MASS J0249−0557AB in our analysis until the accuracy of DR2 parallaxes for close binaries like this can be more carefully vetted. However, we briefly consider here what the difference in our analysis would be if we used the DR2 parallax and proper motion.

The *Gaia* DR2 parallax of 15.11 ± 0.10 mas is 2.6σ lower than our value for 2MASS J0249−0557AB and 1.4σ lower than for 2MASS J0249−0557 c. The *Gaia* DR2 proper motions are 1.2σ higher in R.A. and 2.0σ lower in decl. Using the *Gaia* DR2 parallax and proper motion with the RV from Shkolnik et al. (2017) gives $(U, V, W) = (-11.4 \pm 0.8, -18.81 \pm 0.14, -9.3 \pm 1.1)$ km s^{-1} and $(X, Y, Z) = (-38.2 \pm 0.3, -0.924 \pm 0.006, -54.1 \pm 0.4)$ pc. The most significant difference with our kinematics is in V, which our CFHT astrometry shows is 3 km s^{-1} higher than the mean β Pic group motion but *Gaia* DR2 indicates is 3 km s^{-1} lower. Rerunning our kinematic analysis using *Gaia* DR2 gives a 3D distance from β Pic in proper motion–RV space of 2.0σ, still closer to the mean than 25% of simulated members. Our false-alarm analysis is unchanged because it is based on the selection criteria of the ACRONYM search, which 2MASS J0249−0557AB would still pass.

We also note that the smaller *Gaia* DR2 parallax implies brighter absolute magnitudes for all three components. For 2MASS J0249−0557AB, this would mean bolometric magnitudes of $M_{\rm bol} = 10.51 \pm 0.03$ mag and 10.63 ± 0.03 mag, which in turn would imply a younger age upper limit from the detection of lithium. 2MASS J0249−0557AB would be younger than α Persei (85 ± 10 Myr), where the lithium depletion boundary is at $M_{\rm bol} = 11.31 \pm 0.15$ mag. It would instead be consistent with the next youngest measured lithium depletion boundary in IC 2391 (45 Myr, $M_{\rm bol} = 10.24 \pm 0.15$ mag; Barrado y Navascués et al. 2004). An even younger upper limit on the age would make it correspondingly less likely that the 2MASS J0249−0557 system is a field contaminant rather than a member of the very young β Pic moving group (22 ± 6 Myr). We therefore conclude that the *Gaia* DR2 results are generally consistent with our membership assessment based on our CFHT astrometry. The 0.66 mag brighter J- and K-band absolute magnitudes would also bring all three components of 2MASS J0249−0557ABc closer to the Liu et al. (2016) polynomial relations. 2MASS J0249−0557 c would also lie much closer to β Pic b on the color–magnitude diagram.

The DR2 parallax also implies higher luminosities. The components of 2MASS J0249−0557AB would have $\log(L_{\rm bol}/L_\odot) = -2.32 \pm 0.02$ dex and -2.37 ± 0.02 dex, which would make them more luminous than other known ultracool dwarfs in the β Pic moving group but still normal for a spectral type of M6. Their estimated masses would be somewhat higher, at $75^{+12}_{-11}\ M_{\rm Jup}$ and $69^{+13}_{-9}\ M_{\rm Jup}$, but still consistent with being brown dwarfs. 2MASS J0249−0557 c would have $\log(L_{\rm bol}/L_\odot) = -3.73 \pm 0.02$ dex, that is, 0.05 dex (1.4σ) more luminous than β Pic b, and a mass of $13.2^{+0.4}_{-0.2}\ M_{\rm Jup}$ (1.2σ higher than the mass derived using our CFHT parallax).

4. Discussion

4.1. Implications for the β Pic Moving Group

The 2MASS J0249−0557ABc system increases the total number of ultracool (≥M6) members of the β Pic moving group from seven to ten. Table 5 summarizes these members, as well as other possible members that are lacking either parallax or RV for confirmation, and also those based on proper motion alone. *Gaia* will soon enable a reassessment of all these objects, either directly via high-precision parallaxes and proper motions for the brightest ones or indirectly via an improved census of local moving groups. In the meantime, it is noteworthy that current methods of assessing group membership can still disagree significantly. The 2MASS J0249−0557 system is one such example, as it is not classified as a high-probability ($P \geqslant 90\%$) β Pic member from BANYAN Σ, even though we reaffirm its membership as originally determined by Shkolnik et al. (2017). 2MASS J2208+2921 is a more puzzling case of an object with kinematics that would make it a likely β Pic member according to our analysis but with widely varying probabilities from generalized membership tools, as low as 0.8% from BANYAN Σ (Gagné et al. 2018), so we must conclude that its membership is ambiguous.

2MASS J0249−0557ABc is the first ultracool triple system found in the β Pic moving group. The only other β Pic system containing more than one late-type component is the possible member DENIS J0041−5621AB (integrated-light type M7.5 VL-G; Gagné et al. 2015c; Shkolnik et al. 2017), a 7 au binary with an estimated orbital period of 126 years (Reiners et al. 2010). To our knowledge, no other ultracool triple systems are known in any other young moving groups. The only known binaries are 2MASS J1119−1137AB (Best et al. 2017), which is a likely TWA member, and DENIS J0357−4417AB (Bouy et al. 2003), which is a candidate Tuc-Hor member (Gagné et al. 2014, 2015b). 2MASS J0249−0557ABc is the sixth known substellar triple system, that is, composed entirely of likely brown dwarfs (Bouy et al. 2005; Radigan et al. 2013; Stone et al. 2016; Dupuy & Liu 2017). Compared to the 1950 au separation for 2MASS J0249−0557 c, the other known substellar triples are more compact, with the widest of them (VHS J1256−1257; Stone et al. 2016) having an outer pair separation of 100 au, and the rest having outer separations of 2–27 au.

In contrast to other known young ultracool binaries, 2MASS J0249−0557AB is much tighter (projected separation 2.17 ± 0.22 au at discovery). Its estimated orbital period of ≈8 years makes it likely to yield the first dynamical mass measurement in the β Pic moving group in the substellar regime. In addition to the usual strong tests of substellar models enabled by dynamical masses (e.g., Liu et al. 2008; Dupuy et al. 2010, 2016a; Crepp et al. 2012), this binary will yield the first substellar cooling age (i.e., using luminosity and mass) for a young moving group. Thus, 2MASS J0249−0557AB will enable a unique cross-calibration of substellar evolutionary model tracks by comparing to ages from the lithium-depletion boundary and stellar isochrone methods. The cooling rate of brown dwarfs predicted by evolutionary models has only been independently tested where brown dwarf binaries orbit young stars with gyrochronology-derived ages (Dupuy et al. 2009a,

2014) or where a brown dwarf orbits an older star with a (less precise) isochronal or kinematic age (e.g., Ireland et al. 2008; Bowler et al. 2018). Tests of substellar evolutionary models are especially needed at the young age of β Pic as they are frequently used to infer the physical properties of planetary-mass companions.

4.2. An Unusual System Architecture

2MASS J0249−0557 c ($11.6^{+1.3}_{-1.0}\,M_{\rm Jup}$) is unique among companions at or below the deuterium-fusion boundary given its wide separation (1950 ± 200 au) and the fact that it orbits a very low-mass binary ($48^{+13}_{-12}\,M_{\rm Jup}$ and $44^{+14}_{-11}\,M_{\rm Jup}$). Figure 12 shows the mass ratios of all known directly imaged planetary-mass companions ($\lesssim$13 $M_{\rm Jup}$) as a function of their projected separation. There are only five other companions with similarly wide separations ($\gtrsim 10^3$ au): the AB Dor member GU Psc b (11 ± 2 $M_{\rm Jup}$ at 2000 au; Naud et al. 2014), the Ophiuchus member SR 12 c (13 ± 2 $M_{\rm Jup}$ at 1100 au; Kuzuhara et al. 2011), the young field objects Ross 458 c (9 ± 3 $M_{\rm Jup}$ at 1190 au; Goldman et al. 2010) and TYC 9486-927-1B (12–15 $M_{\rm Jup}$ at 6900 au; Deacon et al. 2016), and the old field object WD 0806−661 b (7.5 ± 1.5 $M_{\rm Jup}$ at 6900 au; Luhman et al. 2012).[19] These host stars range from 0.3 to 2 $M_\odot$ (adopting the progenitor mass for WD 0806−661) and thus represent companion mass ratios of ∼0.03 or much lower, in contrast to the ∼0.1 mass ratio of 2MASS J0249−0557 c. (We adopt the combined mass of 2MASS J0249−0557AB as the host mass for the system.)

Among planetary-mass companions at all separations, few have hosts with such low masses as 2MASS J0249−0557AB, even using its combined mass (50–150 $M_{\rm Jup}$ at 2σ). The two clearest examples are 2MASS J1207−3932 b (5 ± 2 $M_{\rm Jup}$), which orbits a 25 $M_{\rm Jup}$ TWA member (Chauvin et al. 2004), and 2MASS J0441+2301Bb (10 ± 2 $M_{\rm Jup}$), which orbits the 19 ± 3 $M_{\rm Jup}$ tertiary component of a quadruple system in Taurus (Todorov et al. 2010; Kraus et al. 2011; Bowler & Hillenbrand 2015).[20] The slightly higher-mass companions FU Tau B (≈16 $M_{\rm Jup}$; Luhman et al. 2009) and 2MASS J0219−3925B (14 ± 1 $M_{\rm Jup}$; Artigau et al. 2015) orbit a 50 $M_{\rm Jup}$ brown dwarf in Taurus and a 110 $M_{\rm Jup}$ star in Tuc-Hor, respectively.[21] These systems' mass ratios range from 0.13 to 0.5, comparable to but somewhat higher than 2MASS J0249−0557 c. In addition, there are a number of potentially planetary-mass brown dwarfs on close-in orbits of other brown dwarfs with similar or only slightly higher masses that resemble scaled-down binary star systems: SDSS J2249+0044AB (L3+L5; Allers et al. 2010), CFBDSIR J1458+1013AB (T9+Y; Liu et al. 2011), WISE J1217+1626AB (T9+Y0; Liu et al. 2012), WISE J0146+4234AB (T9+Y0; Dupuy et al. 2015a), and 2MASS J1119−1137AB (L7+L7; Best et al. 2017). In short, 2MASS J0249−0557 c is the only planetary-mass companion with both a very wide separation ($>10^3$ au) and relatively high mass ratio ($M_{\rm comp}/M_{\rm host} \gtrsim 0.1$), suggesting that it is more binary-like than planet-like.

4.3. Formation Scenarios

The mass ratio of 2MASS J0249−0557 c to its host binary is consistent with typical stellar triple systems (e.g., Moe & Di Stefano 2017). But even viewed as a very low-mass analog of stellar systems, 2MASS J0249−0557 c is still unusual for the large separation of its tertiary orbit. At a projected separation of 1950 au, it is only weakly bound to 2MASS J0249−0557AB. Although theoretical work suggests that such wide systems can form via the dissolution of the parent cluster (Kouwenhoven et al. 2010), this route is less likely at low component masses, and the progenitor β Pic cluster may never have been dense enough to facilitate capture. Alternatively, turbulent fragmentation models of star formation do predict that objects can form at wide separations (e.g., Offner et al. 2009; Bate 2012). In this scenario, the 2MASS J0249−0557 system would represent the low-mass tail of the star formation process, drawn from an initial mass function that sharply drops toward very low masses (Chabrier 2003). This is consistent with previous surveys for wide-orbit planetary-mass companions that find such systems are rare in young moving groups (e.g., Aller et al. 2016; Naud et al. 2017).

An alternative hypothesis for the origin of 2MASS J0249−0557 c is that it formed in a disk around the binary brown dwarf pair and was scattered outward via dynamical interactions. For the masses and separations involved, this scenario is disfavored for several reasons. First, formation via the bottom-up core accretion process is strongly disfavored based on simple mass requirements. Given the combined mass of the brown dwarf binary host (∼100 $M_{\rm Jup}$), even a disk with a total gas mass equal to the central masses would contain only ∼1 $M_{\rm Jup}$ of solids. This mass is insufficient to trigger runaway gas accretion, even under favorable conditions (Bodenheimer & Pollack 1986; Piso & Youdin 2014). Formation of a tertiary in the disk by gravitational instability instead would also require very high disk masses, which have yet to be observed around brown dwarfs (e.g., Testi et al. 2016). To achieve the current system architecture in this scenario, one must also invoke dynamical interactions between the three objects. While binaries are efficient ejectors of planetary-mass objects (Smullen et al. 2016), the architecture of the 2MASS J0249−0557 system is somewhat disfavored based on energetic arguments. The Keplerian velocity of the tertiary is roughly 3% of the Keplerian velocity of the host binary. Typical scattering encounters would send the tertiary outward at velocities 10× higher than this (Valtonen & Karttunen 2006). Fine-tuning of the interaction would be required to achieve something so marginally bound.

In both scenarios, the fact that the PA of the tertiary companion (228.°649 ± 0.°013) is very close to that of the inner binary (233.°1 ± 0.°3) is most likely a coincidence. Orbit monitoring of the inner binary is needed to determine the actual PA of the orbital node of 2MASS J0249−0557AB, but even if it is aligned with the companion PA, it would be difficult to physically explain orbital alignment over three orders of magnitude in separation.

[19] In order to quote system properties consistently, we use parameters given in Table 1 of the review by Bowler (2016) when available.

[20] 2MASS J0441+2301Bab is itself a wide companion (1800 au) to a pair of 200^{+100}_{-50} $M_{\rm Jup}$ and 35 ± 5 $M_{\rm Jup}$ objects.

[21] VHS J1256−1257 b was originally identified as an 11^{+10}_{-2} $M_{\rm Jup}$ companion to a pair of 65 $M_{\rm Jup}$ objects (Gauza et al. 2015), but Stone et al. (2016) noted the published parallax may have underestimated systematic errors and derived component masses of 73, 73, and 35 $M_{\rm Jup}$ from a spectrophotometric distance, so we exclude it here.

4.4. A Control Sample for Studying Giant Planet Formation

2MASS J0249−0557 c is the first wide-orbit companion ($\gtrsim 10^3$ au) to have properties so similar to a close-in planet from the same moving group, in this case β Pic b (9 au). The existence of a third nearly identical, but free-floating, possible member of the β Pic group 2MASS J2208+2921 would make for a unique trio of planetary-mass objects. There are other well-known analogs; for example, the HR 8799 planets have spectra, colors, and magnitudes similar to that of free-floating objects like PSO J318.5338−22.8603 (Liu et al. 2013) and WISEP J004701.06+680352.1 (Gizis et al. 2015), but no such objects are kinematically associated with the HR 8799 system. 2MASS J0249−0557 c (and possibly 2MASS J2208+2921) are therefore "twins," not merely analogs, of β Pic b because they all formed from the same natal material. Figure 11 illustrates that the colors and magnitudes of these three objects are comparable within the uncertainties, as expected for having similar spectral types and the same age. Similarly, Table 5 shows that they have estimated masses that are consistent within the uncertainties.

If different formation mechanisms produced these objects, then their spectra could contain evidence of their divergent pasts. As noted above, we suspect that 2MASS J0249−0557 c arose from a star-formation-like process of global, top-down gravitational collapse in the same way as the free-floating object 2MASS J2208+2921. On the other hand, β Pic b bears architectural resemblance to planetary systems and thus may have formed via core accretion. Core accretion models and observations of solar system gas giants show substantial metal enrichment (e.g., Stevenson 1982; Bolton et al. 2017). Thus, if β Pic b is a scaled-up gas giant ($\approx$13 $M_{\rm Jup}$), then we may expect to see substantial metal enrichment in its atmosphere. Thorngren et al. (2016) have shown that transiting planets over a wide range of masses ($\sim$0.1–10 $M_{\rm Jup}$) have enhanced metal content with respect to their host stars, with $Z_{\rm pl}/Z_\star \approx 10 \times (M_{\rm pl}/M_{\rm Jup})^{-0.5}$. While this correlation was derived from bulk density measurements, the amount of heavy elements is so large that it implies a significant amount of the metals are likely present in planetary atmospheres as well as their cores.

Some have proposed that planets like β Pic b could form via gravitational instability in a disk (e.g., Boss 2011), though most models suggest that it is unlikely (e.g., Kratter et al. 2010; Rameau et al. 2013). In principle, metallicity enhancement is also possible in this case (Helled et al. 2014), either from dust trapping in spiral arms (Clarke & Lodato 2009) or from accretion of dust and planetesimals (Boley & Durisen 2010). However, in the modern paradigm in which most planetesimals are formed via the streaming instability (Youdin & Goodman 2005), such enhancement may be suppressed. Thus, if β Pic b showed metal enhancement compared to 2MASS J0249−0557 c, this could be a convincing signature of core accretion operating at very high planetary masses. Measuring elemental abundances via molecules in ultracool atmospheres is challenging, but significant progress has already been made on a number of directly imaged planets (e.g., Konopacky et al. 2013; Barman et al. 2015; Skemer et al. 2016; Lavie et al. 2017). The very wide separation of 2MASS J0249−0557 c (40″) and its nearly equatorial decl. will make it amenable to such follow-up observations from nearly any ground-based telescope without needing high-contrast AO.

Formation may also affect the typical rotation rates of planetary-mass objects. The relatively slow rotation of solar system planets is a well-known problem requiring some mechanism to shed angular momentum (e.g., Takata & Stevenson 1996). The equatorial velocity of β Pic b was measured to be 25 km s^{-1} by Snellen et al. (2014), consistent with an extrapolation of the trend among solar system planets for faster rotation to higher masses. The free-floating β Pic moving group member PSO J318.5−22 ($6.5^{+1.2}_{-0.8}$ $M_{\rm Jup}$) is lower in mass than β Pic b and shows a slower equatorial velocity (17.5 ± 1.5 km s^{-1}), as would be expected if it followed the same rotation–mass relation (Allers et al. 2016). The results of Zhou et al. (2016) and Bryan et al. (2018) are also consistent with a single relationship between companions and free-floating objects at planetary masses. However, studies to date have been unable to hold both mass *and* age constant when testing for differences between the rotation of free-floating objects and companions. Fortunately, 2MASS J2208+2921 already has a published rotation period of 3.5 ± 0.2 hr (Metchev et al. 2015) and $v \sin(i) = 40.6^{+1.3}_{-1.4}$ km s^{-1} (Vos et al. 2017), both of which imply significantly more rapid rotation than β Pic b. This is suggestive of the split in behavior that is expected from the slowly rotating solar system planets: objects like β Pic b that spend their early evolution embedded in a disk experience some amount of angular momentum braking, while free-floating objects are more free to spin up. 2MASS J0249−0557 c likely did not form in a disk, so measuring its rotation from variability or $v \sin(i)$ would allow a direct test of this idea.

As directly imaged objects, β Pic b and 2MASS J0249−0557 c provide a new opportunity to test atmospheric compositions and angular momentum evolution for a close-in planet and a very wide companion that share a common mass and age and that formed from the same material.

This work would not have been possible without the excellent, long-running support of CFHT staff past and present, including Loïc Albert, Todd Burdullis, Pascal Fouqué Nadine Manset, Karun Thanjavur, Kanoa Withington, and especially all the queue observers who collected our WIRCam data. We are indebted to Nancy Chanover, Russet McMillan, and Ben Williams of Apache Point Observatory for kindly allowing us to conduct TripleSpec observations during facility engineering time, and Ted Rudyk for assistance with observations. We are grateful to the *W*-band consortium for enabling our SpeX observations, including Loïc Albert, Po-Shih Chiang, Bhavana Lalchand, and especially Jessy Jose for observing assistance. We thank Aaron Rizzuto for helpful discussions. It is also a pleasure to thank the Keck Observatory staff for assistance with the LGS AO observing, including Joel Aycock, Carolyn Jordan, Marc Kassis, Gary Punawai, and Hien Tran. We thank the anonymous referee for a timely review. T.J.D. acknowledges research support from Gemini Observatory. M.C.L. acknowledges support from NSF grant AST-1518339. B.A.B. acknowledges support from STFC grant ST/J001422/1. K.M.K. is supported in part by NSF grant AST-1410174. A.W.M. was supported through Hubble Fellowship grant 51364 awarded by the Space Telescope Science Institute, which is operated by the Association of Universities for Research in Astronomy, Inc., for NASA, under contract NAS 5-26555. E.S. appreciates support from NASA/Habitable Worlds grant NNX16AB62G. Our research has employed NASA's Astrophysical Data System; the SIMBAD database and VizieR catalog access tool, CDS, Strasbourg, France; and James R. A.

Davenport's IDL implementation of the "cubehelix" color scheme (Green 2011). This publication makes use of data products from the *Wide-field Infrared Survey Explorer*, which is a joint project of the University of California, Los Angeles, and the Jet Propulsion Laboratory/California Institute of Technology, funded by the National Aeronautics and Space Administration. This publication utilizes data acquired with SpeX at the IRTF, which is operated by the University of Hawaii under contract NNH14CK55B with the National Aeronautics and Space Administration. Finally, the authors wish to recognize and acknowledge the very significant cultural role and reverence that the summit of Maunakea has always had within the indigenous Hawaiian community. We are most fortunate to have the opportunity to conduct observations from this mountain.

Facilities: Keck:II (LGS AO, NIRC2), CFHT (WIRCam), IRTF (SpeX), ARC (TripleSpec).

ORCID iDs

Trent J. Dupuy https://orcid.org/0000-0001-9823-1445
Michael C. Liu https://orcid.org/0000-0003-2232-7664
Katelyn N. Allers https://orcid.org/0000-0003-0580-7244
Beth A. Biller https://orcid.org/0000-0003-4614-7035
Kaitlin M. Kratter https://orcid.org/0000-0001-5253-1338
Andrew W. Mann https://orcid.org/0000-0003-3654-1602
Evgenya L. Shkolnik https://orcid.org/0000-0002-7260-5821
Adam L. Kraus https://orcid.org/0000-0001-9811-568X
William M. J. Best https://orcid.org/0000-0003-0562-1511

References

Abolfathi, B., Aguado, D. S., Aguilar, G., et al. 2017, ApJS, 235, 42
Alam, S., Albareti, F. D., Allende Prieto, C., et al. 2015, ApJS, 219, 12
Allard, F., Homeier, D., & Freytag, B. 2011, in ASP Conf. Ser. 448, 16th Cambridge Workshop on Cool Stars, Stellar Systems, and the Sun, ed. C. Johns-Krull, M. K. Browning, & A. A. West (San Francisco, CA: ASP), 91
Aller, K. M., Liu, M. C., Magnier, E. A., et al. 2016, ApJ, 821, 120
Allers, K. N., Gallimore, J. F., Liu, M. C., & Dupuy, T. J. 2016, ApJ, 819, 133
Allers, K. N., & Liu, M. C. 2013, ApJ, 772, 79
Allers, K. N., Liu, M. C., Dupuy, T. J., & Cushing, M. C. 2010, ApJ, 715, 561
Artigau, É., Gagné, J., Faherty, J., et al. 2015, ApJ, 806, 254
Baraffe, I., Homeier, D., Allard, F., & Chabrier, G. 2015, A&A, 577, A42
Barman, T. S., Konopacky, Q. M., Macintosh, B., & Marois, C. 2015, ApJ, 804, 61
Barrado y Navascués, D., Stauffer, J. R., & Jayawardhana, R. 2004, ApJ, 614, 386
Bate, M. R. 2012, MNRAS, 419, 3115
Bell, C. P. M., Mamajek, E. E., & Naylor, T. 2015, MNRAS, 454, 593
Bertin, E., & Arnouts, S. 1996, A&AS, 117, 393
Best, W. M. J., Liu, M. C., Dupuy, T. J., & Magnier, E. A. 2017, ApJL, 843, L4
Binks, A. S., & Jeffries, R. D. 2014, MNRAS, 438, L11
Bodenheimer, P., & Pollack, J. B. 1986, Icar, 67, 391
Boley, A. C., & Durisen, R. H. 2010, ApJ, 724, 618
Bolton, S. J., Adriani, A., Adumitroaie, V., et al. 2017, Sci, 356, 821
Boss, A. P. 2011, ApJ, 731, 74
Bouchez, A. H., Le Mignant, D., van Dam, M. A., et al. 2004, Proc. SPIE, 5490, 321
Bouy, H., Brandner, W., Martín, E. L., et al. 2003, AJ, 126, 1526
Bouy, H., Martín, E. L., Brandner, W., & Bouvier, J. 2005, AJ, 129, 511
Bowler, B. P. 2016, PASP, 128, 102001
Bowler, B. P., Dupuy, T. J., Endl, M., et al. 2018, AJ, 155, 159
Bowler, B. P., & Hillenbrand, L. A. 2015, ApJL, 811, L30
Bowler, B. P., Liu, M. C., Mawet, D., et al. 2017, AJ, 153, 18
Bowler, B. P., Liu, M. C., Shkolnik, E. L., & Dupuy, T. J. 2013, ApJ, 774, 55
Bryan, M. L., Benneke, B., Knutson, H. A., Batygin, K., & Bowler, B. P. 2018, NatAs, 2, 138
Burrows, A., Hubbard, W. B., Lunine, J. I., & Liebert, J. 2001, RvMP, 73, 719
Chabrier, G. 2003, PASP, 115, 763
Chauvin, G., Lagrange, A.-M., Dumas, C., et al. 2004, A&A, 425, L29
Chauvin, G., Desidera, S., Lagrange, A.-M., et al. 2017, A&A, 605, L9
Chilcote, J., Pueyo, L., De Rosa, R. J., et al. 2017, AJ, 153, 182
Clarke, C. J., & Lodato, G. 2009, MNRAS, 398, L6
Cohen, M., Wheaton, W. A., & Megeath, S. T. 2003, AJ, 126, 1090
Crepp, J. R., Johnson, J. A., Fischer, D. A., et al. 2012, ApJ, 751, 97
Cruz, K. L., Núñez, A., Burgasser, A. J., et al. 2018, AJ, 155, 34
Cushing, M. C., Rayner, J. T., & Vacca, W. D. 2005, ApJ, 623, 1115
Cushing, M. C., Vacca, W. D., & Rayner, J. T. 2004, PASP, 116, 362
Cutri, R. M., Skrutskie, M. F., van Dyk, S., et al. 2003, 2MASS All Sky Catalog of point sources, (The IRSA 2MASS All-Sky Point Source Catalog, NASA/IPAC Infrared Science Archive. http://irsa.ipac.caltech.edu/applications/Gator/)
Cutri, R. M., Wright, E. L., Conrow, T., et al. 2014, yCat, 2328, 0
Deacon, N. R., Schlieder, J. E., & Murphy, S. J. 2016, MNRAS, 457, 3191
Delorme, P., Gagné, J., Girard, J. H., et al. 2013, A&A, 553, L5
Desrochers, M.-E., Artigau, É., Gagné, J., et al. 2018, ApJ, 852, 55
Dupuy, T. J., Forbrich, J., Rizzuto, A., et al. 2016a, ApJ, 827, 23
Dupuy, T. J., Kratter, K. M., Kraus, A. L., et al. 2016b, ApJ, 817, 80
Dupuy, T. J., & Liu, M. C. 2011, ApJ, 733, 122
Dupuy, T. J., & Liu, M. C. 2012, ApJS, 201, 19
Dupuy, T. J., & Liu, M. C. 2017, ApJS, 231, 15
Dupuy, T. J., Liu, M. C., Bowler, B. P., et al. 2010, ApJ, 721, 1725
Dupuy, T. J., Liu, M. C., & Ireland, M. J. 2009a, ApJ, 692, 729
Dupuy, T. J., Liu, M. C., & Ireland, M. J. 2009b, ApJ, 699, 168
Dupuy, T. J., Liu, M. C., & Ireland, M. J. 2014, ApJ, 790, 133
Dupuy, T. J., Liu, M. C., & Leggett, S. K. 2015a, ApJ, 803, 102
Dupuy, T. J., Liu, M. C., Leggett, S. K., et al. 2015b, ApJ, 805, 56
Faherty, J. K., Burgasser, A. J., Walter, F. M., et al. 2012, ApJ, 752, 56
Faherty, J. K., Riedel, A. R., Cruz, K. L., et al. 2016, ApJS, 225, 10
Filippazzo, J. C., Rice, E. L., Faherty, J., et al. 2015, ApJ, 810, 158
Gagné, J. 2018, jgagneastro/banyan_sigma_idl: BANYAN Σv1.1 (IDL), Zenodo, doi:10.5281/zenodo.1165086
Gagné, J., Burgasser, A. J., Faherty, J. K., et al. 2015a, ApJL, 808, L20
Gagné, J., & Faherty, J. K. 2018, arXiv:1805.11715
Gagné, J., Faherty, J. K., Cruz, K. L., et al. 2015c, ApJS, 219, 33
Gagné, J., Lafrenière, D., Doyon, R., Malo, L., & Artigau, É. 2014, ApJ, 783, 121
Gagné, J., Lafrenière, D., Doyon, R., Malo, L., & Artigau, É. 2015b, ApJ, 798, 73
Gagné, J., Mamajek, E. E., Malo, L., et al. 2018, ApJ, 856, 23
Gaia Collaboration, Brown, A. G. A., Vallenari, A., et al. 2018, arXiv:1804.09365
Gaia Collaboration, Prusti, T., de Bruijne, J. H. J., et al. 2016, A&A, 595, A1
Gauza, B., Béjar, V. J. S., Pérez-Garrido, A., et al. 2015, ApJ, 804, 96
Gizis, J. E., Allers, K. N., Liu, M. C., et al. 2015, ApJ, 799, 203
Goldman, B., Marsat, S., Henning, T., Clemens, C., & Greiner, J. 2010, MNRAS, 405, 1140
Green, D. A. 2011, BASI, 39, 289
Helled, R., & Bodenheimer, P. 2010, Icar, 207, 503
Helled, R., Bodenheimer, P., Podolak, M., et al. 2014, in Protostars and Planets VI (Tucson, AZ: Univ. Arizona Press), 643
Ireland, M. J., Kraus, A., Martinache, F., Lloyd, J. P., & Tuthill, P. G. 2008, ApJ, 678, 463
Ireland, M. J., & Kraus, A. L. 2008, ApJL, 678, L59
Jarrett, T. H., Cohen, M., Masci, F., et al. 2011, ApJ, 735, 112
Kirkpatrick, J. D., Looper, D. L., Burgasser, A. J., et al. 2010, ApJS, 190, 100
Konopacky, Q. M., Barman, T. S., Macintosh, B. A., & Marois, C. 2013, Sci, 339, 1398
Kouwenhoven, M. B. N., Goodwin, S. P., Parker, R. J., et al. 2010, MNRAS, 404, 1835
Kratter, K. M., Murray-Clay, R. A., & Youdin, A. N. 2010, ApJ, 710, 1375
Kraus, A. L., & Hillenbrand, L. A. 2009, ApJ, 704, 531
Kraus, A. L., & Ireland, M. J. 2012, ApJ, 745, 5
Kraus, A. L., Ireland, M. J., Martinache, F., & Hillenbrand, L. A. 2011, ApJ, 731, 8
Kraus, A. L., Shkolnik, E. L., Allers, K. N., & Liu, M. C. 2014, AJ, 147, 146
Kuzuhara, M., Tamura, M., Ishii, M., et al. 2011, AJ, 141, 119
Lagrange, A.-M., Bonnefoy, M., Chauvin, G., et al. 2010, Sci, 329, 57
Lavie, B., Mendonça, J. M., Mordasini, C., et al. 2017, AJ, 154, 91
Lee, J., & Song, I. 2018, MNRAS, 475, 2955

Liu, M. C., Delorme, P., Dupuy, T. J., et al. 2011, ApJ, 740, 108
Liu, M. C., Dupuy, T. J., & Allers, K. N. 2016, ApJ, 833, 96
Liu, M. C., Dupuy, T. J., Bowler, B. P., Leggett, S. K., & Best, W. M. J. 2012, ApJ, 758, 57
Liu, M. C., Dupuy, T. J., & Ireland, M. J. 2008, ApJ, 689, 436
Liu, M. C., Magnier, E. A., Deacon, N. R., et al. 2013, ApJL, 777, L20
Lowrance, P. J., Schneider, G., Kirkpatrick, J. D., et al. 2000, ApJ, 541, 390
Luhman, K. L., Burgasser, A. J., & Bochanski, J. J. 2011, ApJL, 730, L9
Luhman, K. L., Burgasser, A. J., Labbé, I., et al. 2012, ApJ, 744, 135
Luhman, K. L., Mamajek, E. E., Allen, P. R., Muench, A. A., & Finkbeiner, D. P. 2009, ApJ, 691, 1265
Macintosh, B., Graham, J. R., Barman, T., et al. 2015, Sci, 350, 64
Maire, A.-L., Bonnefoy, M., Ginski, C., et al. 2016, A&A, 587, A56
Malo, L., Doyon, R., Lafrenière, D., et al. 2013, ApJ, 762, 88
Mamajek, E. E., & Bell, C. P. M. 2014, MNRAS, 445, 2169
Mann, A. W., Feiden, G. A., Gaidos, E., Boyajian, T., & von Braun, K. 2015, ApJ, 804, 64
Marocco, F., Andrei, A. H., Smart, R. L., et al. 2013, AJ, 146, 161
Marois, C., Macintosh, B., Barman, T., et al. 2008, Sci, 322, 1348
Marois, C., Zuckerman, B., Konopacky, Q. M., Macintosh, B., & Barman, T. 2010, Natur, 468, 1080
Martin, E. C., Mace, G. N., McLean, I. S., et al. 2017, ApJ, 838, 73
Metchev, S. A., Heinze, A., Apai, D., et al. 2015, ApJ, 799, 154
Metchev, S. A., & Hillenbrand, L. A. 2006, ApJ, 651, 1166
Miles-Páez, P. A., Metchev, S., Luhman, K. L., Marengo, M., & Hulsebus, A. 2017, AJ, 154, 262
Moe, M., & Di Stefano, R. 2017, ApJS, 230, 15
Morzinski, K. M., Males, J. R., Skemer, A. J., et al. 2015, ApJ, 815, 108
Naud, M.-E., Artigau, É., Doyon, R., et al. 2017, AJ, 154, 129
Naud, M.-E., Artigau, É., Malo, L., et al. 2014, ApJ, 787, 5
Nielsen, E. L., Liu, M. C., Wahhaj, Z., et al. 2012, ApJ, 750, 53
Offner, S. S. R., Klein, R. I., McKee, C. F., & Krumholz, M. R. 2009, ApJ, 703, 131
Pecaut, M. J., Mamajek, E. E., & Bubar, E. J. 2012, ApJ, 746, 154
Piso, A.-M. A., & Youdin, A. N. 2014, ApJ, 786, 21
Puget, P., Stadler, E., Doyon, R., et al. 2004, Proc. SPIE, 5492, 978
Radigan, J., Jayawardhana, R., Lafrenière, D., et al. 2013, ApJ, 778, 36
Rajan, A., Rameau, J., De Rosa, R. J., et al. 2017, AJ, 154, 10
Rameau, J., Chauvin, G., Lagrange, A.-M., et al. 2013, ApJL, 772, L15
Rayner, J. T., Toomey, D. W., Onaka, P. M., et al. 1998, Proc. SPIE, 3354, 468
Reiners, A., & Basri, G. 2009, ApJ, 705, 1416
Reiners, A., Seifahrt, A., & Dreizler, S. 2010, A&A, 513, L9
Riedel, A. R., Blunt, S. C., Lambrides, E. L., et al. 2017, AJ, 153, 95
Robin, A. C., Reylé, C., Derrière, S., & Picaud, S. 2003, A&A, 409, 523
Rodriguez, D. R., Zuckerman, B., Kastner, J. H., et al. 2013, ApJ, 774, 101
Sallum, S., Follette, K. B., Eisner, J. A., et al. 2015, Natur, 527, 342
Saumon, D., & Marley, M. S. 2008, ApJ, 689, 1327
Schneider, A. C., Windsor, J., Cushing, M. C., Kirkpatrick, J. D., & Shkolnik, E. L. 2017, AJ, 153, 196
Service, M., Lu, J. R., Campbell, R., et al. 2016, PASP, 128, 095004
Shkolnik, E. L., Allers, K. N., Kraus, A. L., Liu, M. C., & Flagg, L. 2017, AJ, 154, 69
Skemer, A. J., Morley, C. V., Zimmerman, N. T., et al. 2016, ApJ, 817, 166
Smullen, R. A., Kratter, K. M., & Shannon, A. 2016, MNRAS, 461, 1288
Snellen, I. A. G., Brandl, B. R., de Kok, R. J., et al. 2014, Natur, 509, 63
Spiegel, D. S., Burrows, A., & Milsom, J. A. 2011, ApJ, 727, 57
Stevenson, D. J. 1982, AREPS, 10, 257
Stone, J. M., Skemer, A. J., Kratter, K. M., et al. 2016, ApJL, 818, L12
Takata, T., & Stevenson, D. J. 1996, Icar, 123, 404
Testi, L., Natta, A., Scholz, A., et al. 2016, A&A, 593, A111
Thorngren, D. P., Fortney, J. J., Murray-Clay, R. A., & Lopez, E. D. 2016, ApJ, 831, 64
Todorov, K., Luhman, K. L., & McLeod, K. K. 2010, ApJL, 714, L84
Torres, C. A. O., Quast, G. R., Melo, C. H. F., & Sterzik, M. F. 2008, in Handbook of Star Forming Regions, Volume II: The Southern Sky ASP Monograph Publications, Vol. 5, ed. B. Reipurth (San Francisco, CA: ASP), 757
Tuthill, P., Lloyd, J., Ireland, M., et al. 2006, Proc. SPIE, 6272, 103
Vacca, W. D., Cushing, M. C., & Rayner, J. T. 2003, PASP, 115, 389
Valtonen, M., & Karttunen, H. 2006, The Three-Body Problem (Cambridge: Cambridge Univ. Press)
van Dam, M. A., Bouchez, A. H., Le Mignant, D., et al. 2006, PASP, 118, 310
van Leeuwen, F. 2007, Hipparcos, the New Reduction of the Raw Data, Vol. 350 (Dordrecht: Springer)
Vos, J. M., Allers, K. N., & Biller, B. A. 2017, ApJ, 842, 78
Wilson, J. C., Henderson, C. P., Herter, T. L., et al. 2004, Proc. SPIE, 5492, 1295
Wizinowich, P. L., Le Mignant, D., Bouchez, A. H., et al. 2006, PASP, 118, 297
Wright, E. L., Eisenhardt, P. R. M., Mainzer, A. K., et al. 2010, AJ, 140, 1868
Yelda, S., Lu, J. R., Ghez, A. M., et al. 2010, ApJ, 725, 331
Youdin, A. N., & Goodman, J. 2005, ApJ, 620, 459
Zhou, Y., Apai, D., Schneider, G. H., Marley, M. S., & Showman, A. P. 2016, ApJ, 818, 176
Zuckerman, B., Rhee, J. H., Song, I., & Bessell, M. S. 2011, ApJ, 732, 61
Zuckerman, B., & Song, I. 2004, ARA&A, 42, 685